properties of composites in terms of the properties of their components, their amounts, and their geometric distribution in the composite. We also discuss the limitations of such expressions.

## 15.5.1 Density and Heat Capacity

Density and heat capacity are two properties that may be predicted rather accurately by a rule-of-mixtures type of relationship, irrespective of the arrangement of one phase in another. The simple relationships predicting these properties of a composite are as follows.

**Density**

The density of a composite is given by the rule-of-mixture equation

$$\rho_c = \rho_m V_m + \rho_r V_r,$$

where $\rho$ designates the density and $V$ represents volume fraction, with the subscripts $c$, $m$, and $r$ denoting the composite, matrix, and reinforcement, respectively.

**Heat capacity**

The heat capacity of a composite is given by the expression

$$C_c = (C_m \rho_m V_m + C_r \rho_r V_r)/\rho_c,$$

where $C$ denotes heat capacity and the other symbols have the significance given in the equation for density.

## 15.5.2 Elastic Moduli

The simplest model for predicting the elastic properties of a fiber/reinforced composite is shown in Figure 15.5. In the longitudinal direction, the composite is represented by a system of "action in parallel" (Figure 15.5(a)). For a load applied in the direction of the fibers, assuming equal deformation in the components, the two (or

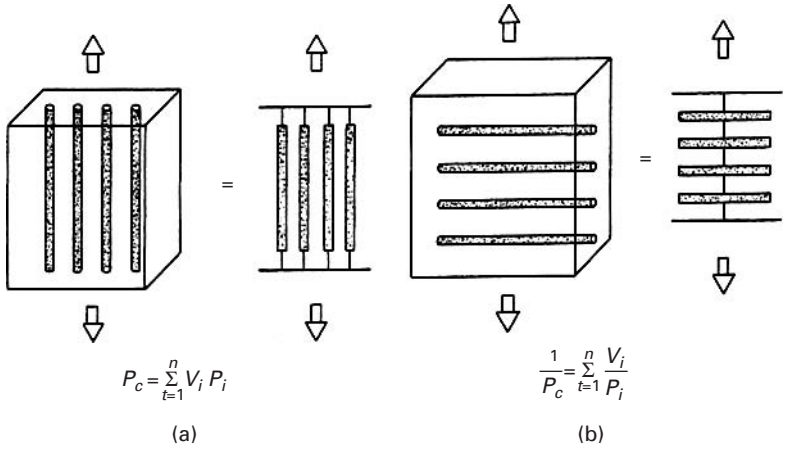


**Fig. 15.5** Simple composite models. (a) Longitudinal response (action in parallel). (b) Transverse response (action in series).

more) phases are viewed as being deformed in parallel. This is the classic case of Voigt's average, in which one has

$$P_c = \sum_{i=1}^{n} P_i V_i, \tag{15.2}$$

where $P$ is a property, $V$ denotes volume fraction, and the subscripts $c$ and $i$ indicate, respectively, the composite and the $i$th component of the total of $n$ components. For the case under study, $n = 2$, and the property $P$ is Young's modulus. We can write, in extended form,

$$E_c = E_f V_f + E_m V_m, \tag{15.3}$$

where the subscripts $f$ and $m$ indicate the fiber and matrix, respectively.

The elastic properties of such unidirectional composites in the transverse direction can be represented by a system of "action in series" (Figure 15.5(b)). Upon loading in a direction transverse to the fibers, then, we have equal stress in the components. This model is equivalent to Reuss's classic treatment. We may write

$$\frac{1}{P_c} = \sum_{i=1}^{n} \frac{V_i}{P_i}. \tag{15.4}$$

Once again, for the case of $n = 2$, and taking the property $P$ to be Young's modulus, we obtain, for the composite,

$$\frac{1}{E_c} = \frac{V_f}{E_f} + \frac{V_m}{E_m}. \tag{15.5}$$

The simple relations expressed Equations 15.4 and 15.5 are commonly referred to as the "rule of mixtures." The reader is warned that this rule is nothing more than a first approximation; more elaborate models have been proposed. The following is a summary of various methods of obtaining composite properties.

- *The mechanics-of-materials method*. This deals with the specific geometric configuration of fibers in a matrix – for example, hexagonal, square, and rectangular – and we introduce large approximations in the resulting fields.
- *The self-consistent field method*. This method introduces approximations in the geometry of the phases. We represent the phase geometry by a single fiber embedded in a material whose properties are equivalent to those of a matrix or an average of a composite. The resulting stress field is thus simplified.
- *The variational calculus method*. This method focuses on the upper and lower limits of the properties of the composite and does not predict those properties directly. Only when the upper and the lower bounds coincide is a particular property determined. Frequently, however, the upper and lower bounds are well separated.
- *The numerical techniques method*. Here we use series expansion, numerical analysis, and finite-element techniques.

The variational calculus method does not give exact results, but provides upper and lower bounds. These results can be used only as indicators of the behavior of the material unless the upper and lower bounds are close enough. Fortunately, this is the case for longitudinal properties. Hill put rigorous limits on the value of $E$ in terms of the bulk modulus in plane strain, $k_p$, Poisson's ratio $\nu$, and the shear modulus $G$ of the two phases.[5] One notes that $k_p$ is the modulus for lateral dilation with zero longitudinal strain ($k_p$ is not equal to $K$) and is given by

$$kp = \frac{E}{2(1-2\nu)(1+\nu)}.$$

According to Hill, the bounds on $E_c$ are

$$\frac{4V_f V_m(\nu_m - \nu_f)^2}{V_f/k_{pm} + V_m/k_{pf} + 1/G_m} \leq E_c - (E_f V_f + E_m V_m)$$
$$\leq \frac{4V_f V_m(\nu_m - \nu_f)^2}{V_f/k_{pm} + V_m/k_{pf} + 1/G_f}. \tag{15.6}$$

It is worth noting that this treatment of Hill does not have restrictions on the form of the fiber, the packing geometry, and so on. We can see, by putting in values in Equation 15.6, that the deviations from the rule of mixtures (Equation 15.3) are rather small, for all practical purposes. For example, take $E_f/E_m = 100$, $\nu_f = 0.25$, $\nu_m = 0.4$. Then the deviation of the Young's modulus of the composite from that predicted by the rule of mixtures is, at most, 2%. For a metallic fiber (e.g., tungsten in a copper matrix), the deviation is less than 1%. Of course, the rule of mixture becomes exact when $\nu_f = \nu_m$.

The transverse properties and the shear moduli are not amenable to such simple reductions. Indeed, they do not obey the rule of mixtures, even to the first approximation. The bounds on them are well spaced. Numerical analysis results show that the behavior of the composite depends on the form and packing of the fiber and on the spacing between fibers.

Unidirectionally reinforced, continuous fiber composites show a linear increase in their longitudinal Young's modulus as a function of the volume fraction of fiber. For materials with a low modulus, such as polymers and metals, reinforcement by high-modulus and high-strength ceramic fibers can result in a significant increase in the composite's elastic modulus and strength. Figure 15.6 shows an example of a linear increase in the longitudinal flexural modulus as a function of the volume fraction of fiber for a glass fiber-reinforced epoxy. In the case of CMCs, an increase in the elastic modulus or strength is rarely the objective, because most monolithic ceramics

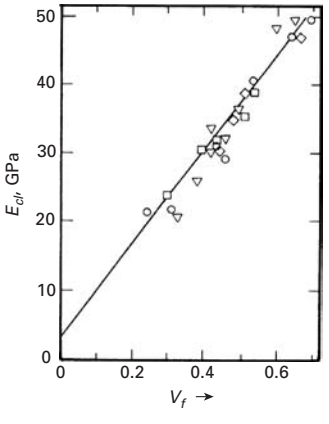


**Fig. 15.6** An example of a linear increase in the longitudinal modulus of the composite, $E_{cl}$, as a function of the volume fraction of fiber for a glass fiber-reinforced epoxy. (After R. D. Adams and D. G. C. Bacon, *J. Comp. Mater.*, 7 (1973) 53.)

[5] R. Hill, *J. Mech. Phys. Solids*, 12 (1964) 199.

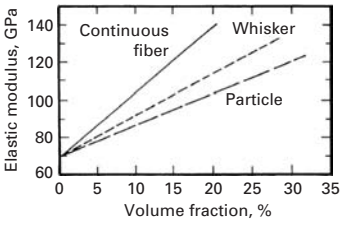


**Fig. 15.7** Schematic of increase in modulus in a composite with reinforcement volume fraction for a different form of reinforcement – continuous fiber, whisker, or particle. Note the loss of reinforcement efficiency as one goes from continuous fiber to particle.

already have very high modulus and strength. However, an increase in the elastic modulus and strength can be a welcome attribute for low-modulus matrix materials – for example, glasses, glass–ceramics, and some crystalline ceramics, such as MgO. Still, the main objective of continuous fiber reinforcement of ceramic matrix materials is to toughen them. In a manner similar to that in PMCs and MMCs, various glass matrix compositions reinforced with carbon fibers have been shown to increase in strength and modulus with the volume fraction of fiber, in accordance with the rule of mixtures. Young's modulus increases linearly with $V_f$, but at a higher $V_f$ it may deviate from linearity, owing to porosity in the matrix and possible misalignment of the fibers.

Particle reinforcement also results in an increase in the modulus of the composite – much less, however, than that predicted by the rule of mixtures. This is understandable, in as much as the rule of mixtures is valid only for continuous fiber reinforcement. A schematic of the increase in modulus in a composite with volume fraction for the same reinforcement, but a different form of reinforcement – continuous fiber, whisker, or particle – is shown in Figure 15.7. This schematic shows the loss of reinforcement efficiency as one goes from continuous fiber to particle.

In sum, we can say that the increase in the longitudinal elastic modulus of a fibrous composite as a function of the reinforcement volume fraction is fairly straightforward. The modulus of a composite is reasonably independent of the reinforcement packing arrangement, as long as all the fibers are parallel. For discontinuous reinforcement, the modulus is also quite independent of the particle clustering, etc. The modulus of a composite does show a dependence on temperature, which enters the picture essentially through the dependence of the matrix modulus on temperature.

## Example 15.3

Consider a glass fiber-reinforced nylon composite. Let the volume fraction of the glass fiber be 65%. The density of glass is 2.1 g $cm^{-3}$, while that of nylon is 1.15 g $cm^{-3}$. Compute the density of the composite. Does it matter whether the glass fiber is continuous?

***Solution:*** The density of the composite is given by

$$\rho_c = \rho_f V_f + \rho_m V_m = 0.65 \times 2.1 + 0.35 \times 1.15 = 1.76\,\mathrm{g\,cm^{-3}}.$$

It does not matter what the exact form of the glass fiber is in the composite. In fact, it could be in the form of equiaxial particles. A rule-of-mixture type of expression is valid for density of all composites, irrespective of the precise geometrical distribution of phases.

## Example 15.4

A carbon fiber reinforced epoxy composite consists of unidirectionally aligned fibers and has $V_f = 65\%$. Calculate the longitudinal and transverse Young's modulus of this composite. $E_f = 200$ GPa, $E_m = 5$ GPa.

***Solution:*** In the longitudinal direction, we have

$$\begin{aligned} E_{cl} &= V_f E_f + (1 - V_f) E_m \\ &= 0.65 \times 200 + 0.35 \times \text{GPa} \\ &= 131.75\,\text{GPa}. \end{aligned}$$

In the transverse direction, we have the expression

$$\frac{1}{E_{ct}} = \frac{V_f}{E_f} + \frac{1 - V_f}{E_m}.$$

Rearranging yields

$$\begin{aligned} E_{ct} &= \frac{E_f E_m}{E_f(1 - V_f) + E_m V_f} \\ &= \frac{200 \times 5}{200 \times 0.35 + 5 \times 0.65} \\ &= 13.65\,\text{GPa}. \end{aligned}$$

Note the high degree of anisotropy. In reality, $E_{ct}$ will be less than the value calculated above because the transverse modulus of carbon fiber is about one-half of the longitudinal modulus value used in the example.

## Example 15.5

Alumina particle (15 volume %) reinforced aluminum composite is used for making some special mountain bicycles. The density of alumina is 3.97 g $cm^{-3}$, while that of aluminum is 2.7 g $cm^{-3}$. Why is this composite used to make the mountain bicycle?

***Solution:*** The alumina–aluminum composite will, of course, be slightly heavier than the unreinforced aluminum. The driving force for using the composite in this case is the enhanced stiffness: $E_{Al_2O_3} = 380$ GPa. while $E_{Al} = 70$ GPa. We can estimate the stiffness of the composite as

$$\begin{aligned} E_{\text{composite}} &= E_{Al_2O_3} V_{Al_2O_3} + E_{Al} V_{Al} \\ &= 380 \times 0.15 + 70 \times 0.85 \\ &= 57 + 59.50 = 116.50\,\text{GPa}. \end{aligned}$$

This estimate is somewhat higher than that realized in practice, because the expression is valid for an unidirectional fiber-reinforced composite, whereas the composite under consideration is a particulate composite. Even so, there is an almost 50% gain in stiffness by adding 15 volume % of alumina particles to aluminum.

### 15.5.3 Strength

Unlike elastic moduli, it is difficult to predict the strength of a composite by a simple rule-of-mixture type of relationship, because strength is a very structure-sensitive property. Specifically, for a composite containing continuous fibers and that is unidirectionally aligned and loaded in the fiber direction, the stress in the composite is written as

$$\sigma_c = \sigma_f V_f + \sigma_m V_m, \tag{15.7}$$

where $\sigma$ is the axial stress, $V$ is the volume fraction, and the subscripts $c$, $f$, and $m$ refer to the composite, fiber, and matrix, respectively. The reason that the rule of mixture does not work for properties such as strength, compared to its reasonable application in predicting properties such as Young's modulus in the longitudinal direction, is the following: The elastic modulus is a relatively structure-insensitive property, so, the response to an applied stress in the composite state is nothing but the volume-weighted average of the individual responses of the isolated components. Strength, on the contrary, is an extremely structure-sensitive property. Thus, synergism can occur in the composite state. Let us now consider the factors that may influence, in one way or the other, composite properties. First, the matrix or fiber structure may be altered during fabrication; and second, composite materials generally consist of two components whose thermomechanical properties are quite different. Hence, these materials suffer residual stresses and/or alterations in structure due to the internal stresses. The differential contraction that occurs when the material is cooled from the fabrication temperature to ambient temperature can lead to rather large thermal stresses, which, in turn, lead a soft metal matrix to undergo extensive plastic deformation. The deformation mode may also be influenced by rheological interaction between the components. The plastic constraint on the matrix due to the large difference in the Poisson's ratio of the matrix compared with that of the fiber, especially in the stage wherein the fiber deforms elastically while the matrix deforms plastically, can alter the stress state in the composite. Thus, the alteration in the microstructure of one or both of the components or the interaction between the components during straining can give rise to synergism in the strength properties of the composite. In view of this, the rule of mixture would be, in the best of the circumstances, a lower bound on the maximum stress of a composite.

Having made these observations about the applicability of the rule of mixture to the strength properties, we will still find it instructive to consider this lower bound on the mechanical behavior of the composite. We ignore any negative deviations from the rule of mixtures due to any misalignment of the fibers or due to the formation of a reaction product between fiber and matrix. Also, we assume that the components do not interact during straining and that these properties in the composite state are the same as those in the isolated state.

Then, for a series of composites with different fiber volume fractions, $\sigma_c$ would be linearly dependent on $V_f$. Since $V_f + V_m = 1$, we can rewrite Equation 15.7 as

$$\sigma_c = \sigma_f V_f + \sigma_m(1 - V_f). \tag{15.8}$$

We can put certain restrictions on $V_f$ in order to have real reinforcement. For this, a composite must have a certain minimum-fiber (continuous) volume fraction, $V_{\min}$. Assuming that the fibers are identical and uniform (that is, all of them have the same ultimate tensile strength), the ultimate strength of the composite will be attained, ideally, at a strain equal to the strain corresponding to the ultimate stress of the fiber. Then, we have

$$\sigma_{cu} = \sigma_{fu} V_f + \sigma'_m(1 - V_f), \quad V_f \geq V_{\min}, \tag{15.9}$$

where $\sigma_{fu}$ is the ultimate tensile of stress of the fiber in the composite and $\sigma'_m$ i s the matrix stress at the strain corresponding to the fiber's ultimate tensile stress. Note that $\sigma'_m$ is to be determined from the stress–strain curve of the matrix alone; that is, it is the matrix flow stress at a strain in the matrix equal to the breaking strain of the fiber. As already indicated, we are assuming that matrix stress–strain behavior in the composite is the same as in isolation. At low volume fractions, if a work-hardened matrix can counterbalance the loss of load-carrying capacity as a result of fiber breakage, the matrix will control the strength of the composite. Assuming that all the fibers break at the same time, in order to have a real reinforcement effect, one must satisfy the relation

$$\sigma_{cu} = \sigma_{fu} V_f + \sigma'_m(1 - V_f) \geq \sigma_{mu}(1 - V_f), \tag{15.10}$$

where $\sigma_{mu}$ is the ultimate tensile stress of the matrix. The equality in this expression serves to define the minimum fiber volume fraction, $V_{\min}$, that must be surpassed in order to have real reinforcement. In that case,

$$V_{\min} = \frac{\sigma_{mu} - \sigma'_m}{\sigma_{fu} + \sigma_{mu} - \sigma'_m}. \tag{15.11a}$$

The value of $V_{\min}$ increases with decreasing fiber strength or increasing matrix strength.

In case we require that the composite strength should surpass the matrix ultimate stress, we can define a critical fiber volume fraction, $V_{\text{crit}}$, that must be exceeded. $V_{\text{crit}}$ is given by the equation

$$\sigma_{cu} = \sigma_{fu} V_f + \sigma'_m(1 - V_f) \geq \sigma_{mu}.$$

In this case,

$$V_{\text{crit}} = \frac{\sigma_{mu} - \sigma'_m}{\sigma_{fu} - \sigma'_m}. \tag{15.11b}$$

$V_{\text{crit}}$ increases with increasing degree of matrix work-hardening ($\sigma_{mu} - \sigma'_m$). Figure 15.8 shows graphically the determination of $V_{\min}$ and $V_{\text{crit}}$. One notes that $V_{\text{crit}}$ will always be greater than $V_{\min}$.

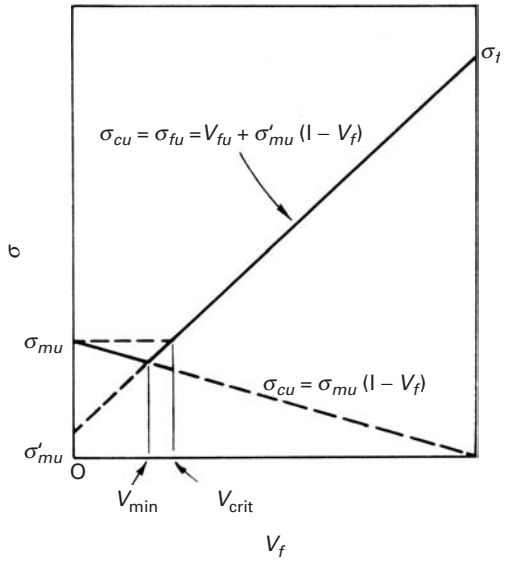


**Fig. 15.8** Determination of $V_{min}$ and $V_{crit}$.

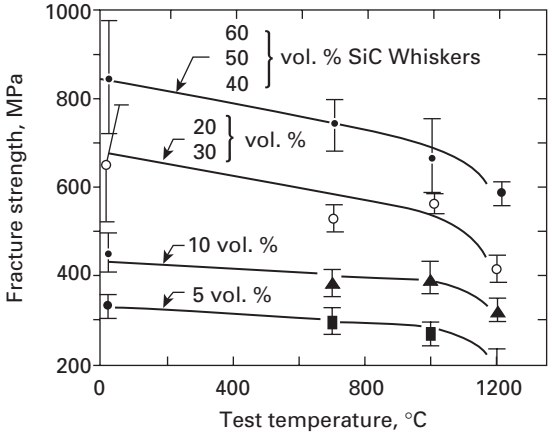


**Fig. 15.9** Increase in strength in silicon carbide whisker–alumina composites as a function of the whisker volume fraction and test temperature. (After G. C. Wei and P. F. Becher, *Am. Ceram. Soc. Bull.*, 64 (1985) 333.)

In general, by incorporating fibers, we can increase the strength of the composite in the longitudinal direction. The strengthening effect in the transverse direction is not significant. Particle reinforcement can result in a more isotropic strengthening, provided that we have a uniform distribution of particles. Carbon, aramid, and glass fibers are used in epoxies to obtain high-strength composites. Such PMCs, however, have a maximum use temperature of about 150 °C. Metal matrix composites, such as silicon carbide fiber in titanium, can take us to moderately high application temperatures. For applications requiring very high temperatures, we must resort to ceramic matrix composites. Silicon carbide whisker reinforced alumina composites show a good combination of mechanical and thermal properties: substantially improved strength, fracture toughness, thermal shock resistance, and high-temperature creep resistance over that of monolithic alumina. Figure 15.9 gives an example of the improvement in

strength in the silicon carbide whisker–alumina composites as a function of the whisker volume fraction and test temperature. Similar results have been obtained with silicon carbide whisker–reinforced silicon nitride composites.

Finally, we should mention the strength of *in situ* composites. In Figure 15.2(c), we showed the microstructure of an *in situ* composite. Such a composite is generally made by the unidirectional withdrawal of heat during the solidification of a eutectic alloy. This controlled solidification allows for one phase to appear in an aligned fibrous form in a matrix of the other phase. The strength $\sigma$ of such an *in situ* metal matrix composites made by directional solidification of eutectic alloys is given by a relationship similar to the Hall–Petch relationship used for grain-boundary strengthening:[6]

$$\sigma = \sigma_0 + k\lambda^{-1/2}.$$

Here $\sigma_0$ is a friction stress term, $k$ is a material constant, and $\lambda$ is the interfiber spacing between rods, or lamellae. It turns out that one can vary $\lambda$ rather easily by controlling the solidification rate $R$, because $\lambda^2 R$ equals a constant. Thus, one can easily control the strength of these *in situ* composites.

### Example 15.6

Consider a uniaxial fiber-reinforced composite of aramid fibers in an epoxy matrix. The volume fraction of fibers is 60%. The composite is subjected to an axial strain of 0.1%. Compute the modulus and strength along the axial direction of the composite corresponding to this starin.

***Solution:*** Both fiber and matrix deform elastically to a strain of 0.1%. Thus, we have

$$\begin{aligned}
\text{longitudinal Young's modulus, } E_{cl} &= E_f V_f + E_m(1 - V_f) \\
&= 140 \times 0.6 + 5 \times 0.4 \\
&= 84 + 2 = 86\,\text{GPa}, \\
\text{longitudinal strength, } \sigma_{cl} &= \sigma_f V_f + \sigma'_m(1 - V_f) \\
&= eE_f V_f + eE_m(1 - V_f) \\
&= e(E_{cl}) = 0.001 \times 86\,\text{GPa}, \\
&= 86\,\text{MPa}.
\end{aligned}$$

### 15.5.4 Anisotropic Nature of Fiber Reinforced Composites

Fiber reinforced composites are highly anisotropic; in particular their mechanical properties are strongly dependent on direction. We derive an expression for the variation in the Young's modulus with the orientation of the fiber for a unidirectionally aligned composite.

[6] H. E. Cline, E. F. Walter, E. F. Koch, and L. M. Osika, *Acta Met.*, 19 (1971) 405.

The generalized Hooke's law may be written as (see Section 2.9)

$$\varepsilon_i = S_{ij}\sigma_j,$$

where $\varepsilon_i$ is the strain, $\sigma_j$ is the stress, $S_{ij}$ is the compliance matrix, and $i$ and $j$ take values from 1 to 6, with summation indicated by a repeated suffix.

The compliances $S_{11}$, $S_{22}$, and $S_{33}$ are reciprocals of the generalized stiffness moduli, and it can be shown (see Chapter 2) that they transform with rotation about a principal axis, say, the $x_3$-axis, according to relations of the type

$$S'_{11} = m^4 S_{11} + n^4 S_{22} + m^2 n^2 (2S_{12} + S_{66}) + 2mn(m^2 S_{16} + n^2 S_{26}), \quad (15.13a)$$

where $m = \cos\theta$, and $n = \sin\theta$, in which $\theta$ is the angle of rotation.

For the discriminating reader, we should point out that this equation follows from the transformation relationship for the fourth rank elasticity tensor:

$$S'_{ijkl} = \ell_{im}\,\ell_{jn}\,\ell_{ko}\,\ell_{lp}\,S'_{mnop}$$

where $\ell_{im}$, $\ell_{jn}$, $\ell_{ko}$, *and* $\ell_{lp}$, are the transformation coefficients. For $S'_{1111}$, we have

$$S'_{1111} = \ell_{lm}\,\ell_{ln}\,\ell_{lo}\,\ell_{lp}\,S'_{mnop}.$$

Care should be exercised when changing from the tensorial to matrix notation (see Section 2.9). For more details on such mathematical operations, the students should consult a text (for example, J. F. Nye. *Physical Properties of Crystals*. London: Oxford University Press, 1975). After converting to matrix notation we arrive at

$$S_{1111} = S_{11}; \quad S_{2222} = S_{22}; \quad 4S_{1212} = S_{66}; \quad 2S_{2212} = S_{26}.$$

For an orthotropic sheet material, such as a prepreg, for which the $x_3$-axis is normal to the plane of the sheet, we have $S_{16} = S_{26} = 0$; then, assuming that the properties in the directions 1 and 2 are the same, Equation 15.13a becomes

$$\begin{aligned} S'_{11} &= (m^4 + n^4)\,S_{11} + m^2 n^2 (2S_{12} + S_{66}) \\ &= \frac{1}{2}S_{11} + \left(\frac{1}{2}S_{12} + \frac{1}{4}S_{66}\right) + \left[\frac{1}{2}S_{11} - \left(\frac{1}{2}S_{12} + \frac{1}{4}S_{66}\right)\right]\cos^2 2\theta. \end{aligned}$$

Now let $E_0$ and $E_{45}$ be Young's modulus for $\theta = 0^\circ$ and $\theta = 45^\circ$, respectively. Then $S_{11} = 1/E_0$ and $\frac{1}{2}S_{11} + \frac{1}{2}S_{12} + \frac{1}{4}S_{66} = 1/E_{45}$. Using these relationships, we get

$$S' = \frac{1}{E_\theta} = \frac{1}{E_{45}} - \left(\frac{1}{E_{45}} - \frac{1}{E_0}\right)\cos^2 2\theta, \quad (15.13b)$$

where $E_\theta$ is the modulus of the composite when the loading direction makes an angle $\theta$ with the fiber direction.

We can also write the compliances $S_{12}$ and $S_{66}$ in terms of the shear modulus $G$ and Poisson's ratio $\nu$ for stresses applied in the

plane of the sheet in the directions 1 and 2. From this, we obtain the relationship

$$\frac{1}{2G} = \frac{1}{E_{45}} - \frac{1}{E_0}(1 - \nu).$$

### 15.5.5 Aging Response of Matrix in MMCs

We have pointed out that the microstructure of a metallic matrix is modified by the presence of a ceramic reinforcement (particle, whisker, or fiber). In particular, a higher dislocation density in the matrix metal or alloy than that in the unreinforced metal or alloy has been observed. The higher dislocation density in the matrix has its origin in the thermal mismatch ($\Delta\alpha$) between the reinforcement and the metal matrix. For example, the thermal mismatch in the case of SiC–Al has a high value of $21 \times 10^{-6}$ K$^{-1}$, which will lead to thermal stress high enough to deform the matrix plastically and thus leave the matrix work-hardened. One expects that the quenching from the solutionizing temperature to room temperature, a change of about 450 °C, will result in a large zone of matrix plastically deformed around each ceramic particle in which the dislocation density will be very high. This high dislocation density will tend to accelerate the aging kinetics of the matrix. Age-hardening treatment can contribute a considerable increment in strength to a precipitation-hardenable aluminum alloy composite. It should be borne in mind that the particle and whisker types of reinforcement, such as SiC, $B_4C$, $Al_2O_3$, etc., are unaffected by the aging process. These particles, however, can affect the precipitation behavior of the matrix quite significantly. The dislocations generated by thermal mismatch form heterogeneous nucleation sites for the precipitates in the matrix during subsequent aging treatments. This in turn alters the precipitation kinetics in the matrix of the composite, compared to the precipitation kinetics in the unreinforced material. Most metal matrix composite work has involved *off-the-shelf* metallic alloys, especially in the case of particle reinforced metal matrix composites. It is important to bear in mind that in such cases using the standard heat treatment practices given in the manuals and handbooks for unreinforced alloys can lead to drastically different results.

### 15.5.6 Toughness

The toughness of a given composite depends on the following factors:

- Composition and microstructure of the matrix.
- Type, size, and orientation of the reinforcement.
- Any processing done on the composite, in so far as it affects microstructural variables (e.g., the distribution of the reinforcement, porosity, segregation, etc.).

Continuous fiber reinforced composites show anisotropy in toughness just as in other properties. The 0° and 90° arrangements of fibers result in two extremes of toughness, while the 0°/90° arrangement

(i.e., alternating laminae of 0° and 90°) gives a sort of pseudo random arrangement with a reduced degree of anisotropy. Using fibers in the form of a braid can make the crack propagation toughness increase greatly due to extensive matrix deformation, crack branching, fiber bundle debonding, and pullout. The composition of the matrix can also have a significant effect on the toughness of a composite: The tougher the matrix, the tougher will be the composite. Thus, a thermoplastic matrix would be expected to provide a higher toughness than a thermoset matrix. In view of the importance of toughness enhancement in CMCs, we offer a summary of the rather extensive effort that has been expended in making tougher ceramics. Some of the approaches to enhancing the toughness of ceramics include the following:

- *Microcracking*. If microcracks form ahead of the main crack, they can cause crack branching, which in turn will distribute the strain energy over a large area. Such microcracking can thus decrease the stress intensity factor at the principal crack tip. Crack branching can also lead to enhanced toughness, because the stress required to drive a number of cracks is more than that required to drive a single crack.
- *Particle toughening*. The interaction between particles that do not undergo a phase transformation and a crack front can result in toughening due to crack bowing between particles, crack deflection at the particle, and crack bridging by ductile particles. Incremental increases in toughness can also result from an appropriate thermal mismatch between particles and the matrix. Taya *et al*. examined the effect of thermal residual stress in a $TiB_2$ particle reinforced silicon carbide matrix composite.[7] They attributed the increased crack growth resistance in the composite vis-a-vis the unreinforced SiC to the existence of compressive residual stress in the SiC matrix in the presence of $TiB_2$ particles.
- *Transformation toughening*. This involves a phase transformation of the second-phase particles at the crack tip with a shear and a dilational component, thus reducing the tensile stress concentration at the tip. In particulate composites, such as alumina containing partially stabilized zirconia, the change in volume associated with the phase transformation in zirconia particles is exploited to obtain enhanced toughness. In a partially stabilized zirconia (e.g., $ZrO_2 + Y_2O_3$), the stress field at the crack tip can cause a stress-induced martensitic transformation in $ZrO_2$ from a tetragonal phase ($t$) to a monoclinic one ($m$); that is,

  $$ZrO_2(t) \rightarrow ZrO_2(m).$$

  This transformation causes an expansion in volume (by approximately 4%) and a shear (0.16). The transformation in a particle at the crack tip results in stresses that tend to close the crack, and

[7] M. Taya, S. Hayashi, A. S. Kobayashi, and H. S. Yoon, *J. Am. Ceram. Soc*., 73 (1990) 1382.

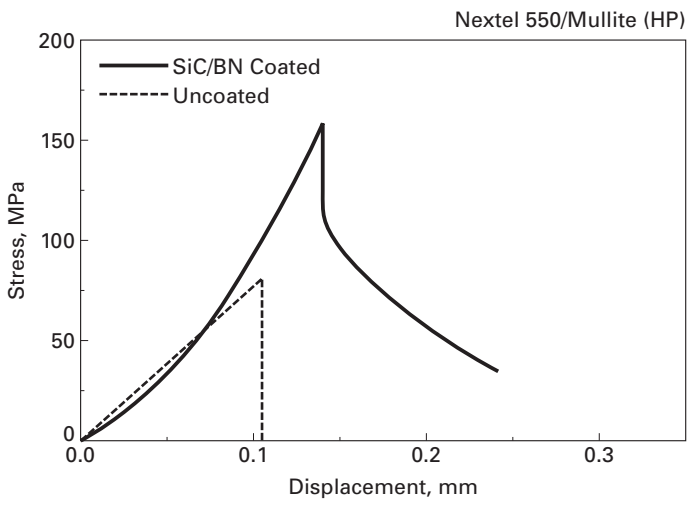


**Fig. 15.10** Stress vs. displacement curves for mullite fiber (Nextel 550)–mullite matrix in three-point bending. The uncoated one refers to the mullite–mullite composite with no interfacial coating, which shows a catastrophic failure. The composite with a double interfacial coating of SiC and BN shows a noncatastrophic failure. (Adapted from K. K. Chawla, Z. R. Xu, and J.-S. Ha, *J. Eur. Ceram. Soc.*, 16 (1996) 293.)

thus a portion of the energy that would go to fracture is spent in the stress-induced transformation. Also, the dilation in the transformed zone around a crack is opposed by the surrounding untransformed material, leading to compressive stresses that tend to close the crack. This results in increased toughness. The phenomenon of transformation toughening was discussed in Chapter 11. Transformation in the wake of a crack can result in a closure force that tends to resist the crack opening displacement. Crack deflection at zirconia particles can also contribute to toughness.

- *Fiber or whisker reinforcement*. Toughening by long fibers or whiskers can bring into play a series of energy-absorbing mechanisms in the fracture process of CMCs and thus allow these materials to tolerate damage.

It appears that the effectiveness of various toughening mechanisms for structural ceramics decreases in the following order: continuous fiber reinforcement; transformation toughening; whiskers, platelets, and particles; microcracking. Many researchers have shown that if we add continuous C or SiC fibers to a glass or ceramic matrix, we can obtain a stress–strain curve of the type shown in Figure 15.10. This curve has the following salient features:

- Damage-tolerant behavior in a composite consisting of two brittle components.
- Initial elastic behavior.
- At a stress $\sigma_0$, the brittle matrix cracks.
- The crack bypasses the fibers and leaves them bridging the crack.
- Under continued loading, we have regularly spaced cracks in the matrix, bridged by the fibers.
- Noncatastrophic failure occurs. Fiber pullout occurs after the peak load, followed by failure of the composite when the fibers fail.

The final failure of the composite does not occur catastrophically with the passage of a single crack; that is, *self-similar* crack propagation

does not occur. Thus, it is difficult to define an unambiguous fracture toughness value, such as a value for $K_{Ic}$.

Figure 15.10 shows the stress vs. displacement curves for mullite fiber (Nextel 550)–mullite matrix. The uncoated one refers to the mullite–mullite composite with no interfacial coating. This composite shows a catastrophic failure. The composite containing a double interfacial coating of SiC and BN shows a noncatastrophic behavior because of the energy expending mechanisms such as interfacial debonding, fiber pullout, etc. come into play during the fracture process. The interfacial coatings provide for easy crack deflection, interfacial debonding, and fiber pullout.

It has been amply demonstrated that incorporation of continuous fibers such as carbon, alumina, silicon carbide, and mullite fibers in brittle matrix materials (e.g., cement, glass, and glass–ceramic matrix) can result in toughening.[8] Not all of these failure mechanisms need operate simultaneously in a given fiber–matrix system, and often, in many composite systems, only one or two of the mechanisms will dominate the total fracture toughness. We discuss this topic further in Section 15.8.

## 15.6 Load Transfer from Matrix to Fiber

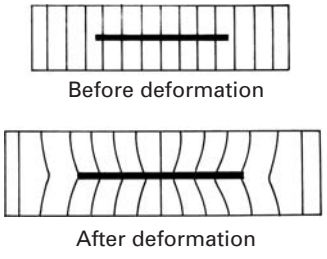


**Fig. 15.11** Perturbation of the matrix stress state due to the presence of fiber.

The matrix has the important function of transmitting the applied load to the fiber. Recall that we emphasized the idea that in fiber reinforced composites, the fibers are the principal load-carrying members. No direct loading of fibers from the ends is admitted. One imagines each fiber to be embedded inside a matrix continuum; the state of stress (and, consequently, that of strain) of the matrix is perturbed by the presence of the fiber (Figure 15.11). When the composite is loaded axially, the axial displacements in the fiber and in the matrix are locally different due to the different elastic moduli of the components. Macroscopically, the composite is deformed homogeneously.

### Example 15.7

The presence of voids in a composite is a serious, but commonly encountered, flaw. Suggest a simple method of determining the void content in a composite.

***Solution:*** A simple method involves determining the density of the composite and getting an accurate estimate of values of the density of the reinforcement and matrix, most likely from the literature. We can write, for the volume of the voids in a composite,

$$V_v = V_c - (V_r + V_m)$$

[8] See, for example, K. K. Chawla, *Ceramic Matrix Composites*, 2nd ed. (Boston: Kluwer Academic, 2003). .

where $V$ is the volume and the subscripts, $v$, $c$, $r$, and $m$ denote the void, composite, reinforcement, and matrix, respectively. Then, knowing the mass and density values, we can write

$$V_v = (M_c/\rho_c) - (V_m/\rho_r + M_m/\rho_m),$$

where $M$ is the mass and $\rho$ is the density, and the subscripts have the significance as before. The density of the composite can then be determined experimentally by Archimedes' method. The amount of reinforcement can be obtained by simply dissolving the matrix in a suitable chemical or by using a thermal method and weighing the residue.

Another simple method of determining the void content is by quantitative microstructural analysis.

The difference in the axial displacements in the fiber and the matrix implies that shear deformations are produced on planes parallel to the fiber axis and in the direction of this axis. These shear deformations are the means by which the applied load is distributed between the two components.

Let us consider the distribution of the longitudinal stress along the fiber–matrix interface. There are two distinct cases: (1) The matrix is elastic and the fiber is elastic, and (2) the matrix is plastic and the fiber is elastic.

### 15.6.1 Fiber and Matrix Elastic

We follow the treatment attributed to Cox.[9] Consider a fiber of length $l$ embedded in a matrix subjected to a strain. Consider a point a distance $x$ from one end of the fiber. It is assumed that (1) there exists a perfect contact between fiber and matrix (i.e., there is no sliding between them) and (2) Poisson's ratios of fiber and matrix are equal. Then the displacement of the point a distance $x$ from one extremity of the fiber can be defined in the following manner; $u$ is the displacement of point $x$ in the presence of the fiber, and $v$ is the displacement of the same point in the absence of the fiber.

The transfer of load from the matrix to the fiber may be written as

$$\frac{dP}{dx} = H(u - v), \tag{15.14a}$$

where $P$ is the load on the fiber and $H$ is a constant to be defined later. ($H$ depends on the geometric arrangement of fibers, the matrix, and their moduli.)

Differentiating Equation 15.14, we obtain

$$\frac{d^2P}{dx^2} = H\left(\frac{du}{dx} - \frac{dv}{dx}\right). \tag{15.14b}$$

[9] H. L. Cox, *Brit. J. App. Phys*., 3(1952) 72.

Now, it follows from the definition that

$$\frac{dv}{dx} = \text{strain in matrix} = e,$$
$$\frac{du}{dx} = \text{strain in fiber} = \frac{P}{A_f E_f}, \tag{15.15}$$

where $A_f$ is the transverse-sectional area of the fiber. From Equations 15.14 and 15.15, we obtain

$$\frac{d^2P}{dx^2} = H\left(\frac{P}{A_f E_f} - e\right). \tag{15.16}$$

A solution of this differential equation is

$$P = E_f A_f e + S \sinh \beta x + T \cosh \beta x \tag{15.17}$$

where

$$\beta = \left(\frac{H}{A_f E_f}\right)^{1/2}. \tag{15.18}$$

The boundary conditions we need to evaluate the constants $S$ and $T$ are

$$P = 0 \text{ at } x = 0 \text{ and } x = \ell.$$

Putting in these values and using the "half-angle" trigonometric formulas, we get the equation

$$P = E_f A_f e \left\{1 - \frac{\cosh \beta[(\ell/2) - x]}{\cosh \beta(\ell/2)}\right\} \quad \text{for } 0 < x < \frac{\ell}{2}. \tag{15.19}$$

or

$$\sigma_f = \frac{P}{A_f} = E_f e \left\{1 - \frac{\cosh \beta[(\ell/2) - x]}{\cosh \beta(\ell/2)}\right\} \quad \text{for} < x < \frac{\ell}{2}. \tag{15.20}$$

The maximum possible value of strain in the fiber is the imposed strain $e$, and thus, the maximum stress is $eE_f$. Hence, as long as we have a sufficiently long fiber, the stress in the fiber will increase from the two ends to a maximum value, $\sigma_f^{\max} = E_f e$. It can readily be shown that the average stress in the fiber will be

$$\bar{\sigma}_f = E_f e \left[1 - \frac{\tanh(\beta\ell/2)}{\beta\ell/2}\right]. \tag{15.21}$$

The variation in the shear stress $\tau$ along the fiber–matrix interface is obtained by considering the equilibrium of forces acting over an element of fiber (with radius $r_f$). Thus,

$$\frac{dP}{dx} dx = 2\pi r_f dx\, \tau. \tag{15.22}$$

$P$ is the tensile load on the fiber and is equal to $\pi r_f^2 \sigma_f$, so

$$\tau = \frac{1}{2\pi r_f} \frac{dP}{dx} = \frac{r_f}{2} \frac{d\sigma_f}{dx}, \tag{15.23}$$

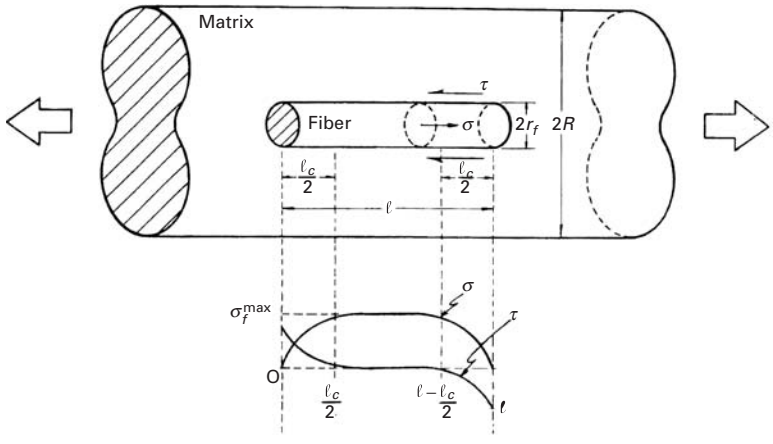


**Fig. 15.12** Load transfer to fiber. Variation in tensile stress $\sigma$ in fiber and shear stress $\tau$ along the interface with the fiber length $\ell$.

or

$$\tau = \frac{E_f r_f e\beta}{2} \frac{\sinh \beta[(\ell/2) - x]}{\cosh \beta(\ell/2)}. \tag{15.24}$$

The variation in $\tau$ and $\sigma_f$ with $x$ is shown in Figure 15.12.

The shear stress $\tau$ in Equation 15.24 will be the smaller of the following two shear stresses:

1. Strength of fiber–matrix interface in shear.
2. Shear yield stress of matrix.

Of these two shear stresses, the one that has a smaller value will control the load transfer phenomenon and should be used in Equation 15.24.

The constant $H$ remains to be determined. An approximate value of $H$ is derived next for a particular geometry. Let the fiber length $\ell$ be much greater than the fiber radius $r_f$, and let $2R$ be the average fiber spacing (center to center). Let $\tau(r)$ be the shear stress in the direction of the fiber axis at a distance $r$ from the axis. Then, at the fiber surface ($r = r_f$),

$$\frac{dP}{dx} = -2\pi r_f \tau(r_f) = H(u - v).$$

Thus,

$$H = -\frac{2\pi r_f \tau(r_f)}{u - v}. \tag{15.25}$$

Let $w$ be the real displacement in the matrix. Then at the fiber–matrix interface, without sliding, $w = u$. At a distance $R$ from the center of a fiber, $w = v$. Considering equilibrium of forces on the matrix between $r_f$ and $R$, we get

$$2\pi r \tau(r) = \text{constant} = 2\pi r_f \tau(r_f),$$

or

$$\tau(r) = \frac{\tau(r_f) r_f}{r}. \tag{15.26}$$

The shear strain $\gamma$ in the matrix is given by $\tau(r) = G_m r$, where $G_m$ is the matrix shear modulus. Then

$$\gamma = \frac{dw}{dr} = \frac{\tau(r)}{G_m} = \frac{\tau(r_f)r_f}{G_m r}. \tag{15.27}$$

Integrating from $r_f$ to $R$, we get

$$\Delta w = \frac{\tau(r_f)r_f}{G_m} \ln\left(\frac{R}{r_f}\right). \tag{15.28}$$

But, by definition,

$$\Delta w = v - u = -(u - v). \tag{15.29}$$

Then

$$\frac{\tau(r_f)\, r_f}{u - v} = -\frac{G_m}{\ln(R/r_f)}. \tag{15.30}$$

From Equations 15.25 and 15.30, we get

$$H = \frac{2\pi G_m}{\ln(R/r_f)}, \tag{15.31}$$

and from Equation 15.18, we obtain an expression for the load transfer parameter:

$$\beta = \left(\frac{H}{E_f A_f}\right)^{1/2} = \left[\frac{2\pi G_m}{E_f A_f \ln(R/r_f)}\right]^{1/2}. \tag{15.32}$$

Note that the greater the value of $G_m/E_f$, the more rapid is the increase in fiber stress from the two ends.

The foregoing analysis is an approximate one – particularly with regard to the evaluation of the load transfer parameter $\beta$. More exact analysis give similar results and differ only in the value of $\beta$. In all the analyses, however, $\beta$ is proportional to $\sqrt{G_m/E_f}$, and the differences occur only in the term involving the fiber volume fraction, $\ln(R/r_f)$.

### 15.6.2 Fiber Elastic and Matrix Plastic

It should be clear from the preceding discussion that, in order to load high-strength fibers to their maximum strength in the matrix, the shear strength must correspondingly be large. A metallic matrix will flow plastically in response to the high shear stress developed. Should the fiber–matrix interface be weaker, it will fail first. Plastic deformation of a matrix implies that the shear stress at the fiber surface, $\tau(r_f)$, will never go above $\tau_y$, the matrix shear yield strength (ignoring any work-hardening effects). In such a case, we get, from an equilibrium of forces, the equation

$$\sigma_f \pi \frac{d^2}{4} = \tau_y \pi d \frac{\ell}{2},$$

or

$$\frac{\ell}{d} = \frac{\sigma_f}{2\tau_y}.$$

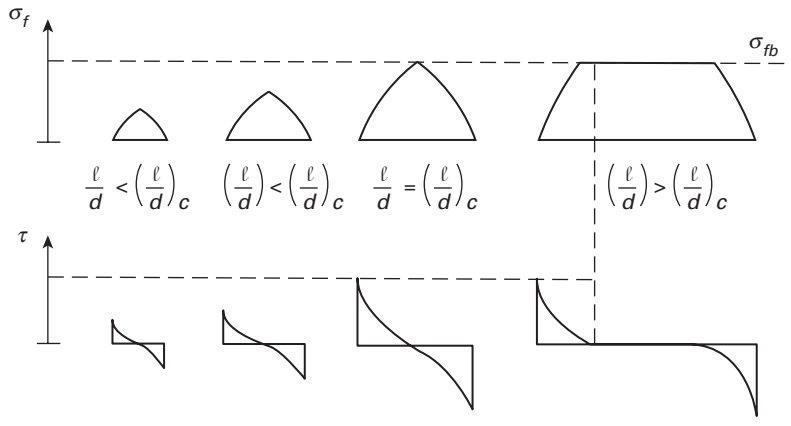


**Fig. 15.13** Variation in the fiber load transfer length as a function of the aspect ratio $\ell/d$.

We consider $\ell/2$, and not $\ell$, because the fiber is being loaded from both ends. If the fiber is sufficiently long, it should be possible to load it to its breaking stress, $\sigma_{fb}$, by means of load transfer through the matrix flowing plastically around it. Let $(\ell/d)_c$ be the minimum fiber length-to-diameter ratio necessary to accomplish this. We call this ratio $\ell/d$ the aspect ratio of the fiber and $(\ell/d)_c$ the critical aspect ratio necessary to attain the breaking stress of the fiber, $\sigma_{fb}$. Then we can write

$$\left(\frac{\ell}{d}\right)_c = \frac{\sigma_{fb}}{2\tau_y}. \tag{15.33}$$

Or we can think of a critical fiber length $\ell_c$ for a given fiber diameter $d$:

$$\frac{\ell_c}{d} = \frac{\sigma_{fb}}{2\tau_y}. \tag{15.34}$$

Thus, the fiber length $\ell$ must be equal or greater than $\ell_c$ for the fiber to be loaded to its maximum stress. If $\ell < \ell_c$, the matrix will flow plastically around the fiber and will load it to a stress in its central portion given by

$$\sigma_f = 2\tau_y \frac{\ell}{d} < \sigma_{fb}. \tag{15.35}$$

This is shown in Figure 15.13. An examination of the figure shows that, even for $\ell/d > (\ell/d)_c$, the average stress in the fiber will be less than the maximum stress to which it is loaded in its central region. In fact, we can write, for the average fiber stress,

$$\begin{aligned}\bar{\sigma}_f &= \frac{1}{\ell}\int_0^{\ell} \sigma_f dx \\ &= \frac{1}{\ell}[\sigma_f(\ell - \ell_c) + \phi\sigma_f\ell_c] \\ &= \frac{1}{\ell}[\sigma_f\ell - \ell_c(\sigma_f - \phi\sigma_f],\end{aligned}$$

or

$$\bar{\sigma}_f = \sigma_f \left(1 - \frac{1-\phi}{\ell/\ell_c}\right), \tag{15.36}$$

where $\phi\sigma_f$ is the average stress in the fiber over a portion $\ell_c/2$ of its length at both the ends. We can thus regard $\phi$ as a load transfer function where value will be precisely 0.5 for an ideally plastic matrix (i.e., the increase in stress in the fiber over the portion $\ell_c/2$ will be linear).

### Example 15.8

(a) Consider an alumina fiber reinforced polymer matrix composite. If the strength of the fiber is 1 GPa and the fiber–matrix interface has a shear strength of 10 MPa, compute the critical fiber length $\ell_c$. Take the diameter of the alumina fiber to be 10 μm.

(b) The composite in Part a is made of short (1-cm-long), but aligned, alumina fibers. Assuming that each fiber is loaded from both ends in a linear manner, compute the average stress in the fiber in this composite.

***Solution:*** (a) Critical length:

$$\ell_c/d = \sigma_{fb}/2\tau_i = 1,000/(2 \times 10) = 50,$$
$$\ell_c = 50 \times 10\,\mu m = 0.5mm.$$

(b) Average fiber stress:
From the solution to Part a, we have

$$\ell/\ell_c = 10/0.5 = 20,$$
$$\bar{\sigma}_f = \sigma_f[1 - (1-\phi)/(\ell/\ell_c)]$$
$$= 1{,}000[1 - (1 - 0.5)/20] = 1{,}000(1 - 0.025) = 975\,\text{MPa}.$$

## 15.7 Fracture in Composites

Fracture is a complex subject, even in monolithic materials. (See Chapters 7–9.) Undoubtedly, it is even more complex in composite materials. A great variety of deformation modes can lead to failure in a composite. The operative failure mode will depend, among other things, on loading conditions and the particular composite system. The microstructure has a very important role in the mechanics of rupture of a composite. For example, the fiber diameter, its volume fraction and alignment, damage due to thermal stresses that may develop during fabrication or service – all these factors can contribute to, and directly influence, crack initiation and propagation. A multiplicity of failure modes can exist in a composite under different loading conditions.

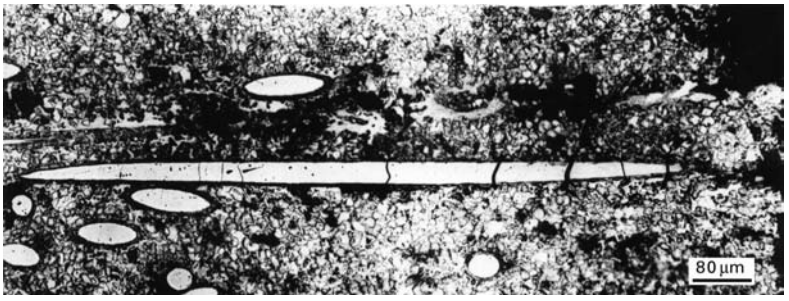


**Fig. 15.14** Optical micrograph showing multiple fracture of tungsten fibers in an Fe–Cu matrix.

### 15.7.1 Single and Multiple Fracture

In general, the two components of a composite will have different values of strain to fracture. When the component that has the smaller breaking strain fractures, the load carried by this component is thrown on to the other one. If the latter component, which has a higher strain to fracture, can bear the additional load, the composite will show multiple fracture of the brittle component (the one with smaller fracture strain); eventually, a particular transverse section of composite becomes so weak, that the composite is unable to carry the load any further, and it fails.

Let us consider the case of a fiber reinforced composite in which the fiber fracture strain is less than that of the matrix. Then the composite will show a single fracture when

$$\sigma_{fu} V_f > \sigma_{mu} V_m - \sigma'_m V_m, \tag{15.37}$$

where $\sigma'_m$ is the matrix stress corresponding to the fiber fracture strain and $\sigma_{fu}$ and $\sigma_{mu}$ are the ultimate tensile stresses of the fiber and matrix, respectively. This equation says that when the fibers break, the matrix will not be in a condition to support the additional load, a condition that is commonly encountered in composites of high $V_f$, brittle fibers, and a ductile matrix. All the fibers break in more or less one plane, and the composite fails in that plane.

If, on the other hand, we have a system that satisfies the condition

$$\sigma_{fu} V_f < \sigma_{mu} V_m - \sigma'_m V_m, \tag{15.38}$$

the fibers will be broken into small segments until the matrix fracture strain is reached. An example of this type of breakage is shown in Figure 15.14, an optical micrograph of an Fe–Cu matrix containing a small volume fraction of W fibers.

In case the fibers have a fracture strain greater than that of the matrix (an epoxy resin reinforced with metallic wires), we would have a multiplicity of fractures in the matrix, and the condition for this may be written as

$$\sigma_{fu} V_f > \sigma_{mu} V_m - \sigma'_m V_f, \tag{15.39}$$

where $\sigma'_f$ is now the fiber stress corresponding to the matrix fracture strain.

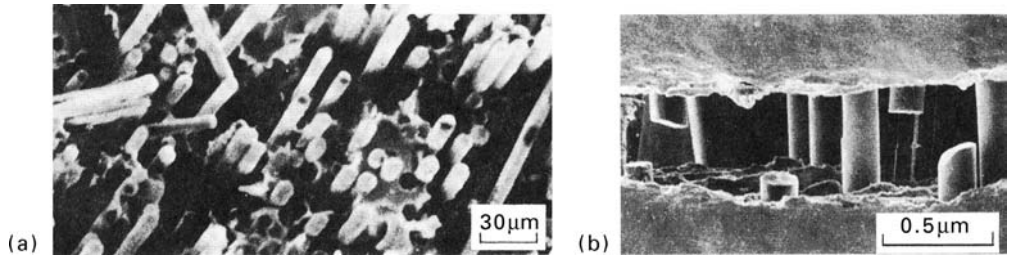


**Fig. 15.15** Scanning electron micrographs of fracture in composites, showing the fiber pullout phenomenon. (a) Carbon fiber/polyester. (b) Boron fiber/aluminum 6061.

### 15.7.2 Failure Modes in Composites

Two failure modes are commonly encountered in composites:

1. The fibers break in one plane, and, the soft matrix being unable to carry the load, the composite failure will occur in the plane of fiber fracture. This mode is more likely to be observed in composites that contain relatively high fiber volume fractions and fibers that are strong and brittle. The latter condition implies that the fibers do not show a distribution of strength with a large variance, but show a strength behavior that can be characterized by the Dirac delta function.
2. When the adhesion between fibers and matrix is not sufficiently strong, the fibers may be pulled out of the matrix before failure of the composite. This fiber pullout results in the fiber failure surface being nonplanar.

More commonly, a mixture of these two modes is found: fiber fracture together with fiber pullout. Fibers invariably have defects distributed along their lengths and thus can break in regions above or below the crack tip. This leads to separation between the fiber and the matrix and, consequently, to fiber pullout with the crack opening up. Examples are shown in Figure 15.15.

One of the attractive characteristics of composites is the possibility of obtaining an improved fracture toughness behavior together with high strength. Fracture toughness can be defined loosely as resistance to crack propagation. In a fibrous composite containing a crack transverse to the fibers, the crack propagation resistance can be increased by doing additional work by means of any or all of the following:

- Plastic deformation of the matrix.
- The presence of weak interfaces, fiber–matrix separation, and deflection of the crack.
- Fiber pullout.

It would appear that debonding of the fiber–matrix interface is a prerequisite for phenomena such as crack deflection, crack bridging by fibers, and fiber pullout. It is of interest to develop some criteria for interfacial debonding and crack deflection. Crack deflection at an interface between materials of identical elastic constants (i.e., the same material joined at an interface) has been analyzed on the basis of the strength of the interface. The deflection of the crack along

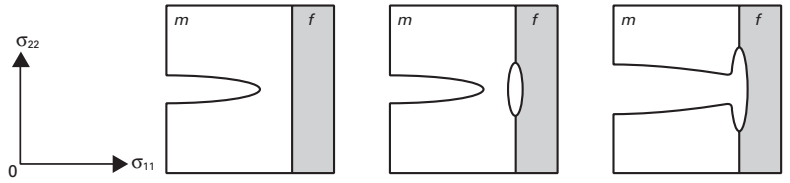


**Fig. 15.16** Fracture of weak interface in front of crack tip due to transverse tensile stress; *m* and *f* indicate the matrix and fiber, respectively. (After J. Cook and J. E. Gordon, *Proc. Roy. Soc. (London)*, A 228 (1964) 508.)

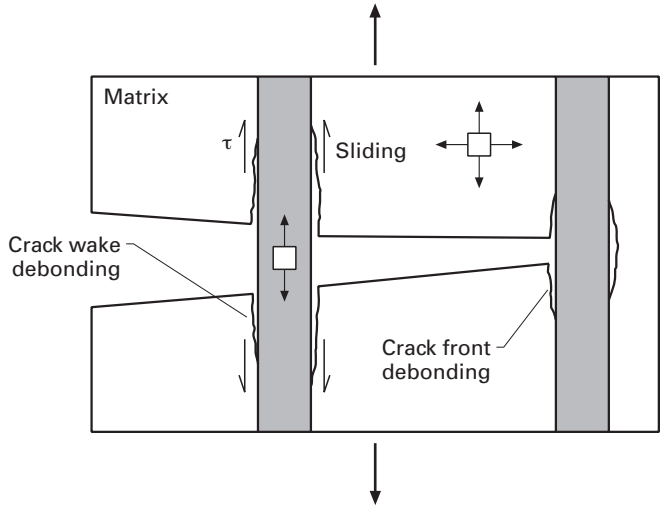


**Fig. 15.17** Crack front and crack wake debonding in a fiber reinforced composite.

an interface or the separation of the fiber–matrix interface is an interesting mechanism of augmenting the resistance to crack propagation in composites. Cook and Gordon analyzed the stress distribution in front of a crack tip and concluded that the maximum transverse tensile stress $\sigma_{11}$ is about one-fifth of the maximum longitudinal tensile stress $\sigma_{22}$. They suggested, therefore, that when the ratio $\sigma_{22}/\sigma_{11}$ is greater than 5, the fiber–matrix interface in front of the crack tip will fail under the influence of the transverse tensile stress, and the crack would be deflected 90° from its original direction. That way, the fiber–matrix interface would act as a crack arrester. This is shown schematically in Figure 15.16. The improvement in fracture toughness due to the presence of weak interfaces has been confirmed qualitatively.

Another treatment of this subject is based on a consideration of the fracture energy of the constituents.[10] Two materials that meet at an interface are more than likely to have *different* elastic constants. This mismatch in moduli causes shearing of the crack surfaces, which leads to a mixed-mode stress state in the vicinity of an interface crack tip involving both the tensile and shear components. This, in turn, results in a mixed-mode fracture, which can occur at the crack tip or in the wake of the crack. Figure 15.17 shows crack front and

[10] See M. Y. He and J. W. Hutchinson, *J. App. Mech.*, 56 (1989) 270; A. G. Evans and D. B. Marshall, *Acta Met.*, 37 (1989) 2567.

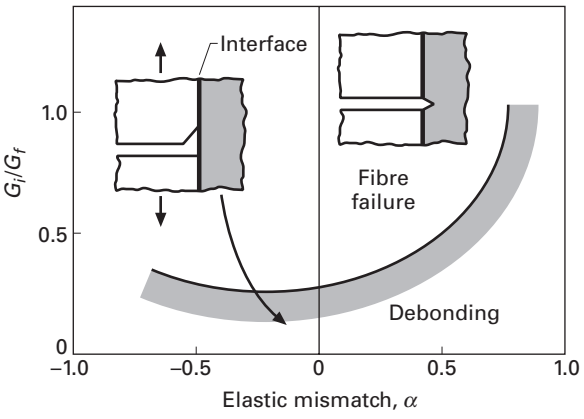


**Fig. 15.18** The ratio of the interface fracture toughness to that of fiber, $G_i/G_f$, vs. the elastic mismatch $\alpha$. Interfacial debonding occurs under the curve, while for conditions above the curve, the crack propagates through the interface.

crack wake debonding in a fiber reinforced composite. Because of the mixed-mode fracture, a single-parameter description by the critical stress intensity factor $K_{Ic}$ will not do; instead, one needs a more complex formalism of fracture mechanics to describe the situation. In this case, the parameter $K$ becomes scale sensitive, but the critical strain energy release rate $G_{Ic}$ is not a scale-sensitive parameter. $G$ is a function of the phase angle $\psi$, which, in turn, is a function of the normal and shear loading. For the opening mode, or mode I, $\psi = 0^\circ$, while for mode II, $\psi = 90^\circ$. One needs to specify both $G$ and $\psi$ to analyze the debonding at the interface. Without going into the details, we present here the final results of such an analysis, in the form of a plot of $G_i/G_f$ vs. $\alpha$, where $G_i$ is the mixed-mode interfacial fracture energy of the interface, $G_f$ is the mode-I fracture energy of the fiber, and $\alpha$ is a measure of the elastic mismatch between the matrix and the reinforcement, defined as

$$\alpha = \left( \frac{\bar{E}_1 - \bar{E}_2}{\bar{E}_1 + \bar{E}_2} \right), \tag{15.40}$$

where

$$\bar{E} = \frac{E}{1 - \nu^2}. \tag{15.41}$$

The plot in Figure 15.18 shows the conditions under which the crack will deflect along the interface or propagate through the interface into the fiber. For all values of $G_i/G_f$ below the shaded boundary, interface debonding is predicted. For the special case of zero elastic mismatch (i.e., for $\alpha = 0$), the fiber–matrix interface will debond for $G_i/G_f$ less than about 0.25. Conversely, for $G_i/G_f$ greater than 0.25, the crack will propagate across the fiber. In general, for elastic mismatch, with $\alpha$ greater than zero, the minimum interfacial toughness required for interface debonding increases (i.e., high-modulus fibers tend to favor debonding). One shortcoming of this analysis is that it treats the fiber and matrix as isotropic materials; this is not always true, especially for carbon fiber.

Gupta *et al*.[11] derived strength and energy criteria for crack deflection at a fiber–matrix interface for several composite systems, taking due account of the anisotropic nature of the fiber. They used an experimental technique – spallation by means of a laser Doppler displacement interferometer – to measure the tensile strength of a planar interface. Through this technique, these researchers have tabulated the required values of the interface strength and fracture toughness for delamination in a number of ceramic, metal, intermetallic, and polymer matrix composites.

## 15.8 Some Fundamental Characteristics of Composites

Composite materials are not like any other common type of material. They are inherently different from monolithic materials, and consequently, these basic differences must be taken into account when one designs or fabricates any article from composite materials. In what follows, we give a brief description of some of the fundamental characteristics of composites.

### 15.8.1 Heterogeneity

Composite materials are inherently heterogeneous, consisting as they do of two components of different elastic moduli, different mechanical behavior, different expansion coefficients, and so on. For this reason, the analysis of, and the design procedures for, composite materials are quite intricate and complex, compared to those for ordinary materials. The structural properties of composites are functions of:

**1.** The properties of their components.
**2.** The geometric arrangement of their components.
**3.** The interface between the components.

Given two components, we can obtain a great variety of properties by manipulating items 2 and 3.

### 15.8.2 Anisotropy

In general, monolithic materials are reasonably isotropic; that is, their properties do not show any marked preference for any particular direction. The unidirectional composites are anisotropic due to their very nature. Once again, the analysis and design of composites should take into account this strong directionality of properties – properties that cannot be specified without any reference to some direction. Figure 15.19 shows, schematically, the elastic moduli of a monolithic material and a composite as a function of fiber orientation $\theta$. (See Section 15.5.4.) A monolithic material (e.g., Al) is an isotropic

[11] V. Gupta, J. Yuan, and D. Martinez, *J. Am. Ceram. Soc*., 76 (1993) 305.

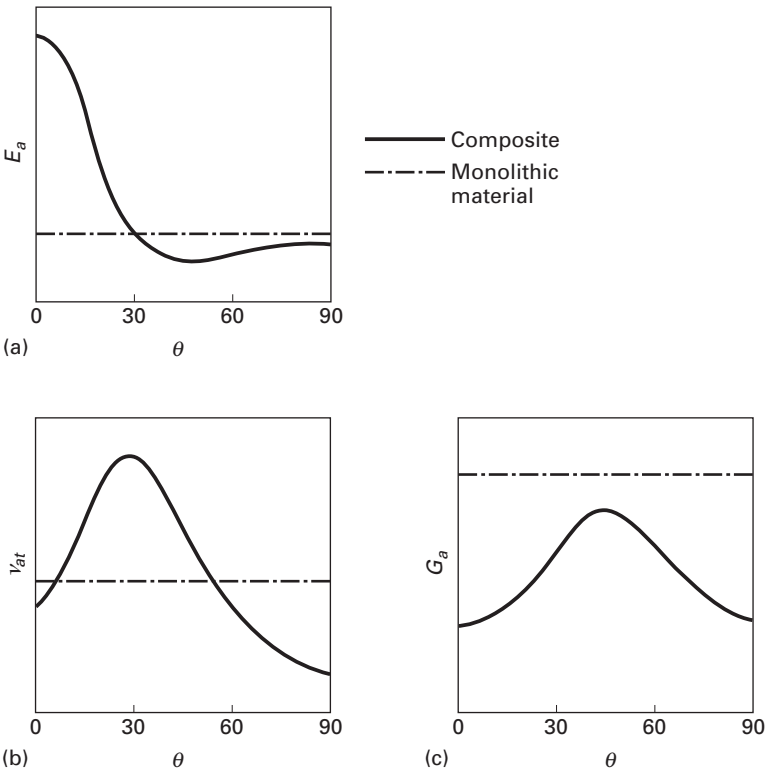


**Fig. 15.19** Schematic of variation in elastic moduli of a fiber composite and a monolithic material with the angle of reinforcement. (a) $E_a$ is the axial Young's modulus (b) $\nu_{at}$ is the principal Poisson's ratio, and (c) $G_a$ is the axial shear modulus.

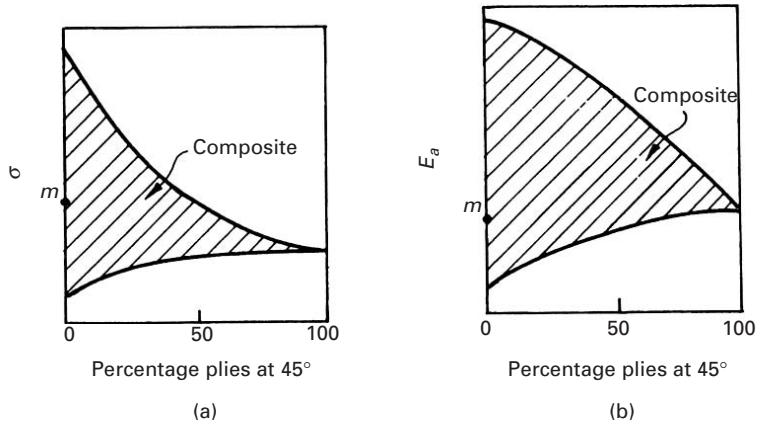


**Fig. 15.20** Schematic of a performance chart of a composite.

material; therefore, its moduli do not vary with the angle of testing, and the graphs are horizontal.

For an ordinary material (say, aluminum), the designer only needs to open a manual and find one unique value of strength or one unique value of the modulus of the material. But for fiber reinforced composite materials, the designer has to consult performance charts representing the strength and the modulus of the various composite systems. (See Figure 15.20.)

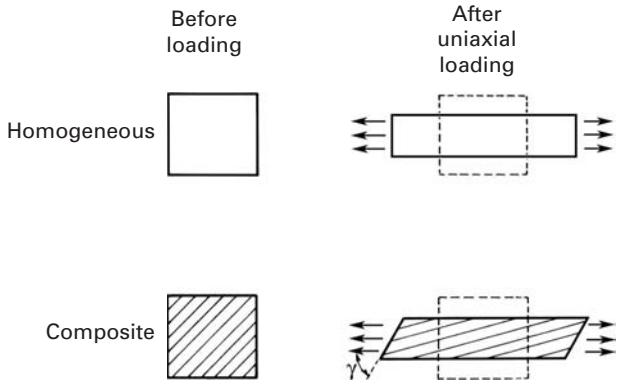


**Fig. 15.21** Shear coupling in a fiber composite

Ordinary materials, such as aluminum or steel, can be represented by a fixed point, indicated by *m* in Figure 15.20. For a composite material, however, there does not exist a unique combination of these properties. Instead, the composite contains a system of properties and must be represented by an area instead of a point. We call these graphs "carpet plots." These plots give modulus or strength in terms of proportion of plies at different angles. The highest point on the graph represents the longitudinal properties of the composite, while the lowest point represents transverse properties. The important point to make is that, depending on the stacking of plies in a composite and the appropriate quantity of fiber, the characteristics of the composite can be varied. In other words, composites can be tailormade, in accord with the final objective.

### 15.8.3 Shear Coupling

The properties of a composite are very sensitive functions of the fiber orientation. They display what is called *shear coupling*: shear strains produced by axial stress and axial strains produced by shear stress. (See Figure 15.21.) In response to a uniaxially applied load, an isotropic material produces only axial and transverse strains. In fiber reinforced composites, however, a shear strain $\gamma$ is also produced in response to an axial load, because the fibers tend to align themselves in the direction of the applied load. This shear distortion can be eliminated if one makes a *cross-ply* composite – a composite containing an equal number of parallel fibers, alternately aligned at a given angle and at a complementary angle with respect to the loading axis (Figure 15.22). That is, we have the various layers in a composite arranged at $\pm\ \theta$ degrees to the loading axis, and thus, the shear distortion due to one layer is compensated for by an equal and opposite shear distortion due to the other. However, this balance occurs only in two dimensions, whereas the real-life composites are three-dimensional materials. This leads to an "edge effect" in which the individual layers deform differently under tension and in the neighborhood of the free edges, giving rise to out-of-plane shear and bending. The stacking sequence of the various layers in the composite is important. For example, in a laminate composite consisting of fibers

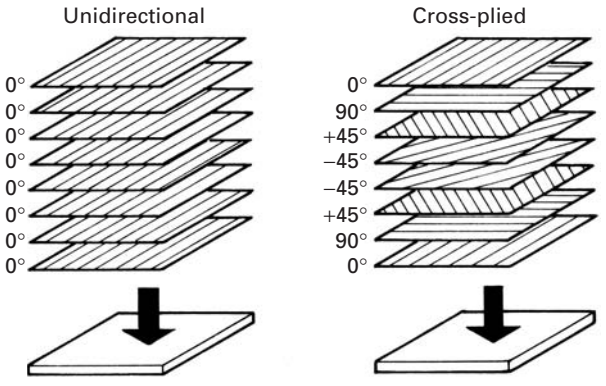


**Fig. 15.22** Unidirectional and cross-plied composites.

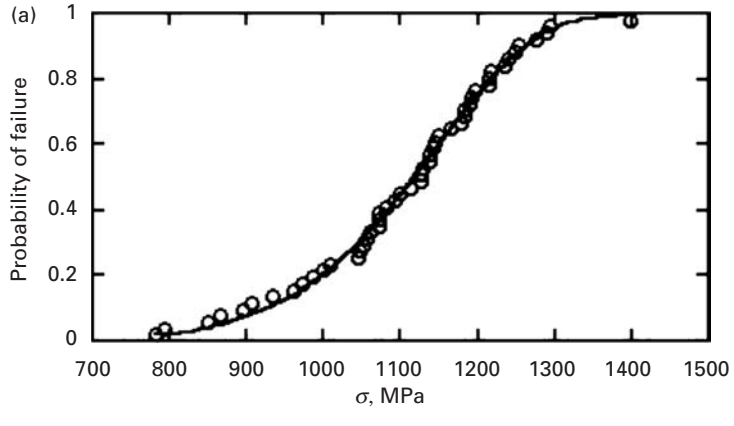


**Fig. 15.23** Probability of failure versus strength (Weibull) plot of tensile strength of a carbon fiber–epoxy composite. (Courtesy of B. Atadero and V. Karbhari.)

at $+90^\circ$, $+45^\circ$, $-45^\circ$, $-45^\circ$, $+45^\circ$, and $+90^\circ$, subjected to an in-plane tensile stress, there occur compressive stresses in the direction of thickness, in the vicinity of the edges. Should the same composite have the sequence $+45^\circ$, $-45^\circ$, $+90^\circ$, $+90^\circ$, $-45^\circ$, $+45^\circ$, however, these stresses in the direction of thickness are of a tensile nature and thus tend to delaminate the composite, clearly an undesirable effect.

### 15.8.4 Statistical Variation in Strength

The strength of a composite can show significant variation from specimen to specimen. Thus, care has to be exercised when tests are conducted and strength is quoted. As an example, Figure 15.23 shows the results of 50 tensile tests carried out on a carbon fiber–epoxy matrix composite. The strength varied from 800 to 1400 MPa, a considerable spread. The Weibull modulus is 9.9, and $\sigma_m$ is 1,160 MPa. The Weibull modulus is on the same order as the one for ceramics. The experimental results follow a Weibull distribution, which is represented by the continuous line in Figure 15.23.

## 15.9 Functionally Graded Materials

There is a good deal of interest in making materials that are graded in some respect. The gradient may be of the chemical composition, density, or coefficient of thermal expansion of the material, or it may involve microstructural features – for example, a particular arrangement of second-phase particles or fibers in a matrix. Such materials are called *functionally graded materials*, and the acronym FGM is commonly applied to them in the literature. Strictly speaking, though, the term "graded material" ought to be enough to convey the meaning; that is, the word "functionally" is redundant. The idea, however, is a very general one, viz., instead of having a step function, say, in composition at an interface, we should have a gradually varying composition from component *A* to component *B*. Figure 15.24 shows schematically the microstructure of a functionally graded material. Such a graded interface can be very useful in ameliorating high mechanical and thermal stresses. The concept of a functionally graded material is applicable to any material, polymer, metal, or ceramic.[12]

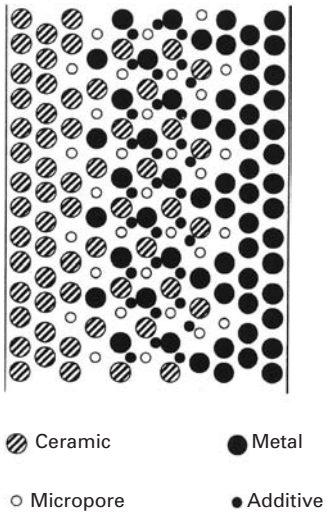


**Fig. 15.24** Schematic of a functionally graded material between a ceramic on the left-hand side and a metal on the right-hand side. Also shown are micropores and additives.

## 15.10 Applications

It is convenient to divide the applications of all composites into aerospace and nonaerospace categories. In the category of aerospace applications, low density coupled with other desirable features, such as a tailored thermal expansion and conductivity, and high stiffness and strength, are the main drivers. Performance, rather than cost, is an important item as well. We next give a brief description of various applications of composites.

### 15.10.1 Aerospace Applications

Reduction in the weight of a component is as major driving force for any application in the aerospace field. The Boeing 757 and 767 jets were the first large commercial aircraft to make widespread use of structural components made of PMCs. About 95% of the visible interior parts in Boeing 757 and 767 cabins are made from nonconventional materials. Most of the fuselage of a Boeing 787 is made of carbon/epoxy while a considerable part of Airbus 380 uses GLARE composites (see Sec. 15.11). One of the main reasons for the decision to use such materials was the steadily dropping price of carbon fibers. Similarly, there has been an increasing use of composites in aircraft, including helicopters, used by defense services. Weight and cost savings are the driving forces for these applications. Consider, for example, the Sikorsky H-69 helicopter. For this helicopter, manufacturing the conventional fuselage, of metal construction, is very labor intensive. In comparison, the composite fuselage, of carbon, aramid, and

[12] See B. Ilschner, *J. Mech. Phys. Solids*, 44 (1996) 647; S. Suresh and A. Mortensen, *Intl. Mater. Rev.*, 42 (1997) 85.

glass fiber–epoxy, has much fewer parts, assemblies, and fasteners. PMCs are also lighter and cheaper to use than metals in the manufacture of fuselages. The use of lighter composites in aircraft results in energy savings: For a given aerodynamic configuration of an aircraft, there is a direct correlation between the weight of the airplane and fuel consumption. Weight savings resulting from the use of new, lighter materials lead to great increases in fuel economy.

In examining the applications of composites in space, it should be recognized that environment of space is not benign. Among the hazardous items that may be encountered in space are orbital debris, meteorites, and atomic oxygen. It appears that metal matrix composites can withstand the space environment better than polymer matrix composites. In the Hubble telescope, pitch-based continuous carbon fiber reinforced aluminum was used for waveguide booms because this composite is very light and has a high elastic modulus and a low coefficient of thermal expansion.

Other aerospace applications of MMCs involve the replacement of light, but toxic, beryllium by various composites. For example, in the U.S. Trident missile, beryllium has been replaced by an $SiC_p$/Al composite, which is also used in aircraft electronic equipment racks.

CMCs can lead to potential improvements in aircraft, helicopters, missiles, reentry modules of spacecraft, and other aerospace vehicles. Projected skin temperatures in future hypersonic aircraft are over 1600 °C. Other parts, such as radomes, nose tips, leading edges, and control surfaces, will have only slightly lower temperatures. Currently, one uses sacrificial, non-load-bearing thermal protection CMC materials on load-bearing components made of conventional materials. With the use of CMCs, one can have load-bearing components that are reusable at operating temperatures.

### 15.10.2 Nonaerospace Applications

Polymer composites based on aramid, carbon, and glass fibers are routinely used in civil construction and in marine and sporting goods. Applications in the sporting goods industry have burgeoned, all the way from tennis rackets to fishing poles to a whole variety of equipment used in downhill as well as cross-country skis, boots, poles, gloves, etc. The main advantages that the use of composites brings to the sporting goods industry are safety, less weight, and higher strength than conventional materials. Ski poles made of polymer composites are lighter and stiffer than aluminum poles. Frequently, hybrid composites are used, such as carbon fibers laid over a small sleeve of aramid.

Composites are also used in rifle stocks for biathlons because both weight and strength are important in the rifles, which may have to be carried over distances of up to 20 km.

The automobile industry is a major user of PMCs, mainly because of the cost advantage over other types of composites. One of the important applications of MMCs in the automotive area is in the diesel piston crown. This application involves the incorporation of

short fibers of alumina or alumina plus silica into the crown. The conventional diesel engine piston has an Al–Si casting alloy with a crown made of nickel cast iron. The replacement of the nickel cast iron by an aluminum matrix composite resulted in a lighter, more abrasion-resistant, and cheaper product. Yet another application of MMCs is in the automobile engine of the Honda *Prelude*. In the conventional automobile, the major part of the engine, and also the heaviest part, is the cast iron engine block. In the general quest for high performance combined with a light vehicle, the cast iron engine block has been replaced by light aluminum alloy in some automobiles, resulting in a weight reduction of 15–35 kg. But even in these aluminum engines, the liners are generally made of cast iron. This is because cast iron has superior sliding characteristics (pistons sliding in the cylindrical bores) than aluminum alloys do. The Honda Motor Company has developed an aluminum engine (used in the *Prelude*), with cylinder liners made of alumina- and carbon-fiber reinforced aluminum. The most important characteristic for this application is resistance against sliding. Seizure occurs when the coefficient of friction increases very rapidly. According to the researchers at Honda, a hybrid composite consisting of alumina and carbon fibers gave the best results. This was attributed to the self-lubricating properties of carbon fiber and the sliding resistance of alumina fiber. In composites containing only alumina fibers, when a scratch appeared, it easily worsened. In the case of hybrid alumina and carbon fibers in Al, the scratch did not grow. Particulate metal matrix composites – especially light ones such as aluminum and magnesium – also find applications in automotive and sporting goods. In this regard, it is important to remember that the price per kilogram becomes the driving force for the application.

An interesting application, led by 3M Co., involving continuous alumina fibers in aluminium matrix is in the form of a composite conductor, which is used in power-line cables. These new cables are capable of transmitting two or three times more electricity than the conventional power-line cables of the same diameter without additional weight or the need for more towers. The objective is to increase the amperage capacity of the existing power-line structures with no additional easements. Congestion is a key issue facing the power transmission grid in the USA. These new cables have a core that consists of composite (continuous alumina fiber in an aluminium matrix). The core is wrapped by aluminium–zirconium alloy conductor wires. Figure 15.25 shows the cross section of one such cable. This 3M conductor cable, also known as aluminum composite conductor reinforced (ACCR) cable, is light weight; consequently it sags less than the conventional power lines. It can be used to span difficult terrains such as wide rivers, lakes, or canyons. Because of their light weight, such cables are also able to withstand winter snow storms that cause accumulation of ice on the power lines, resulting in their snapping.

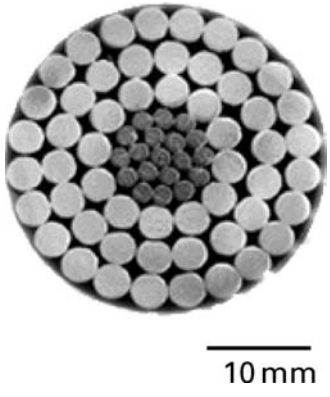


**Fig. 15.25** Cross section of an aluminium composite conductor reinforced (ACCR) cable. The central wires consist of continuous alumina fibers in an aluminium matrix composite while the outer wires are made of Al–Zr alloy. (Courtesy of 3M Co.)

Copper-based composites having Nb, Ta, or Cr as the second phase in a discontinuous form are of interest for certain applications

requiring high thermal conductivity and high strength. Sometimes we refer to these composites as Cu–*X* composites, where *X*, which is insoluble in copper at room temperature, forms the second phase. One specific example is a high heat-flux application in the thrust chambers of rocket engines. Cu–*X* systems are very useful for processing such composites. At room temperature, the second phase appears in a dendritic form, which can be converted into a filamentary or ribbon form by mechanical working. Note that the ribbon morphology is thermodynamically unstable at high temperatures, because the ribbons tend to form spheroids with time, as a function of temperature.

Conventional commercial superconductors are referred to as *niobium-based superconductors* because Nb–Ti and $Nb_3Sn$ are superconducting materials. These conventional superconductors are nothing but copper matrix composites.

An area in which CMCs have found application is that of cutting tools. Silicon carbide whisker reinforced alumina ($SiC_w/Al_2O_3$) is used as a cutting-tool insert for high-speed cutting of superalloys. For example, in the cutting of Inconel 718, $SiC_w/Al_2O_3$ composite tools perform three times better than conventional ceramic tools and eight times better than cemented carbides.

Carbon–carbon composites are used as implants, as well as for internal fixation of bone fractures, because of their excellent biocompatibility. They are also used for making molds for hot pressing. Carbon–carbon molds can withstand higher pressures and offer a longer service life than does polycrystalline graphite. However, their high cost limits them to aerospace and other specialty applications. The low oxidation resistance of carbon–carbon composites is a serious limitation, but is not a problem for short-term applications such as shields, rocket nozzles, and reentry vehicles.

## 15.11 Laminated Composites

The abalone shell is a natural laminar or laminated composite based on $CaCO_3$. It possesses unique strength and toughness properties. In Chapter 1 we showed a picture of the structure (Figure 1.30). The flexural strength of the abalone shell is approximately 80 MPa; in comparison, the flexural strength of monolithic $CaCO_3$ is close to 10 MPa. The fracture toughness of abalone is in the 4–10 MPa $m^{1/2}$ range, whereas that of $CaCO_3$ is approximately 1 MPa $m^{1/2}$. Figure 15.26 shows the dramatic improvement in mechanical strength made possible by the organization of calcium carbonate into layers with thickness of approximately 0.5 μm. The same figure shows the improvement in properties obtained when $Al_2O_3$ is arranged in layers with Al ($Al_2O_3$/Al) and when $B_4C$ is used to form a laminate with Al ($B_4C$/Al).

Figure 15.27(a) shows the construction of tiles forming the nacreous portion of abalone. This structure resembles a "brick and

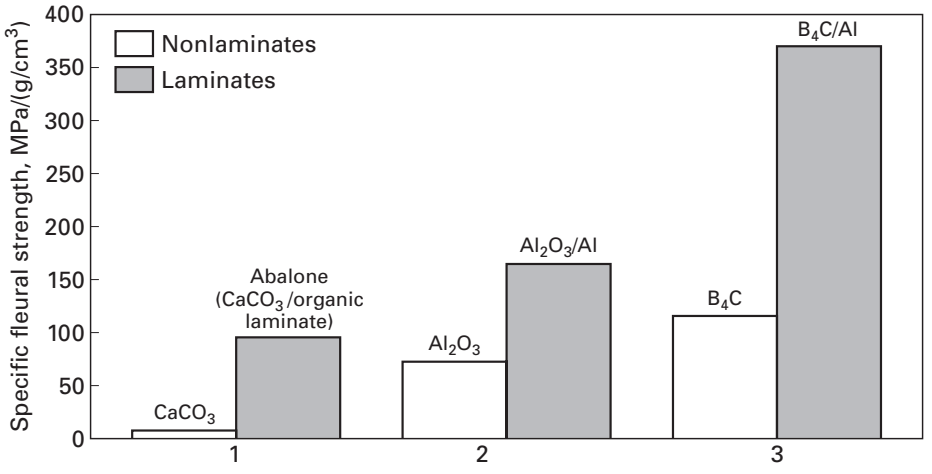


**Fig. 15.26** Flexural strength for selected monolithic and laminated materials. (Adapted from M. Sarikaya, *Micr. Res. Tech*., 27 (1994) 371.)

mortar" structure where aragonite (an orthorhombic form of $CaCO_3$) is represented by "bricks" bound together by organic material ("mortar"). Again, the thick bands are made of aragonite and the thin layers in between the aragonite plates are an organic "glue." This laminated structure of aragonite and organic material is the primary reason for the toughness of abalone. When abalone fractures under application of load, the resulting crack will follow a tortuous path that requires considerable energy to grow. Figure 15.27(b) shows the fracture surface. We see that the tiles are actually pulled out. These tiles slide past each other and the glue between them provides the resistance. This pullout action is shown in the sequence depicted in Figure 15.27(c).

Several laminated composites are commercially available. A laminated composite made of two glass sheets bonded with poly(vinyl butryal), PVB, is used as a transparent safety glass material in a variety of applications, the most important being the automotive windshield. Bilayer or bimetallic compostes are commonly used as switches. Some of the newer laminated composites are made by stacking alternate layers of a fiber reinforced polymer composite and monolithic metallic sheet. Examples include ARALL (aramid aluminum laminate) which consists of alternate layers of aramid fiber–epoxy and aluminum sheet and GLARE, which consists of alternate layers of glass fiber–epoxy and aluminum sheet. Figure 15.28 shows schematically such composites. They are also known as fiber metal laminates. Such composites have very high specific stiffness and strength. They are also more resistant to cyclic fatigue. Figure 15.29 shows the microstructure (SEM and TEM) of a laminated composite of aluminum and silicon carbide made by physical vapor deposition on a silicon substrate. It has mechanical properties vastly superior to those of individual components. These laminated composites are examples of bioinspired materials, where the same toughening principle is used as does nature in the abalone shell.

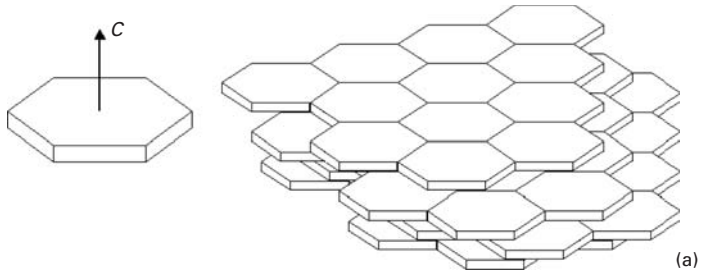


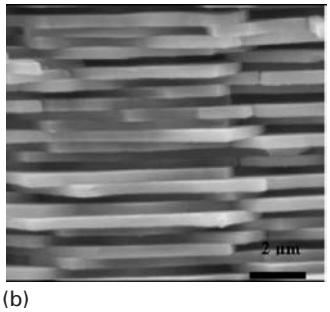


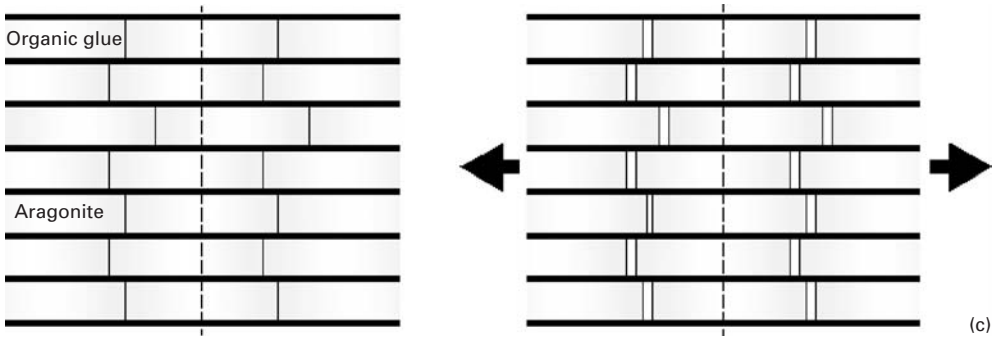


**Fig. 15.27** (a) Schematic showing an arrangement of tiles; (b) SEM of a fractured surface of abalone showing pullout of tiles; (c) schematic showing how pullout of tiles occurs through shear of organic layer that acts as glue. (Courtesy of A. Lin.)

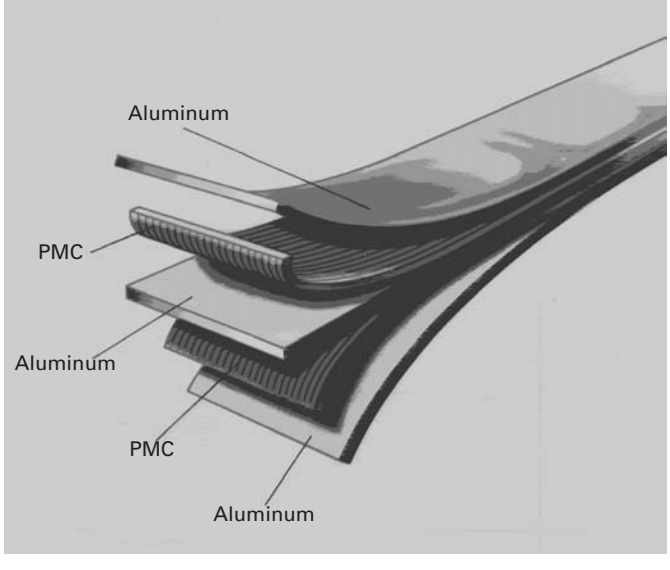


**Fig. 15.28** Schematic of a metal–polymer matrix composite (PMC) such as *Arall* or *Glare*.

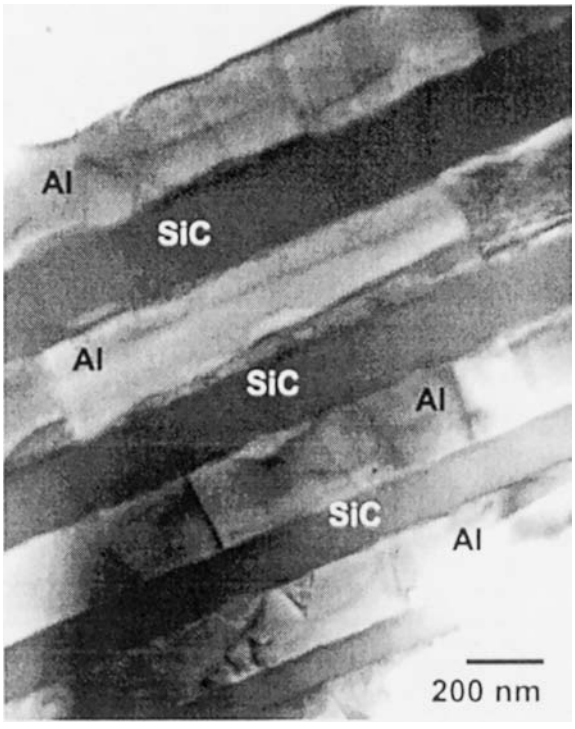


(a)

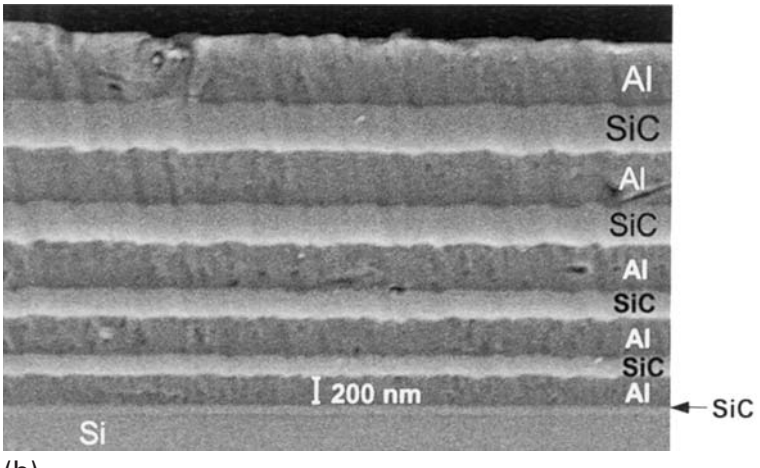


(b)

**Fig. 15.29** Cross section of a laminate consisting of aluminum and silicon carbide: (a) SEM; (b) TEM. (From X. Deng, K. K. Chawla, M. Koopman, and J. P. Chu, *Adv. Eng. Mater.*, 7 (2005) 1.)

## Suggested Reading

K. K. Chawla. *Composite Materials: Science and Engineering*, 2nd ed. New York, NY: Springer, 1998.

K. K. Chawla. *Ceramic Matrix Composites*, 2nd ed. Boston, MA: Kluwer Academic, 1993.

K. K. Chawla. *Fibrous Materials*. Cambridge, U.K.: Cambridge University Press, 1998.

N. Chawla and K. K. Chawla, *Metal Matrix Composites*. New York, NY: Springer, 2006.
T. W. Clyne and P. Withers. *Metal Matrix Composites*. Cambridge, U.K.: Cambridge University Press, 1994.
L. N. Phillips, ed. *Design with Advanced Composite Materials*. London: The Design Council, 1989.
S. Suresh, A. Needleman, and A. M. Mortensen, eds. *Fundamentals of Metal Matrix Composites*. Stoneham, MA: Butterworth–Heinemann, 1993.

## Exercises

**15.1** Describe some composite materials that occur in nature. Describe their structure and properties.

**15.2** To promote wettability and avoid interfacial reactions, protective coatings are sometimes applied to fibers. Any improvement in the behavior of a composite will depend on the stability of the layer of coating. The maximum time $t$ for the dissolution of this layer can be estimated by the diffusion distance

$$x \approx \sqrt{Dt},$$

where $D$ is the diffusivity of the matrix in the protective layer. Making an approximation that the matrix diffusion in the protective layer can be represented by self-diffusion, compute the time required for a 0.1-μm-thick protective layer on the fiber to be dissolved at $T_m$ and $0.75T_m$, where $T_m$ is the matrix melting point in kelvin. Assume a reasonable value of $D$ for self-diffusion in metals, taking into account the variation in $D$ with temperature.

**15.3** A fibrous form represents a higher energy form vis-a-vis a spherical form. Hence, a fibrous phase produced by unidirectional solidification of an euectic will tend to form spheroids because such a change of shape results in a decrease in the surface energy of the material. Compute the energy released when a 10-cm-long, 20-μm-diameter fiber becomes spheroidal. The specific surface energy of the fibrous phase is 500 m $Jm^{-2}$.

**15.4** One can obtain two-dimensional isotropy in a fiber composite plate by having randomly oriented fibers in the plane of the plate. Show that the average in-plane modulus is

$$\bar{E}_\theta = \frac{\int_0^{\pi/2} E_\theta d\theta}{\int_0^{\pi/2} d\theta}.$$

Plot $E_\theta/E_{11}$ versus $V_f$ for fiber reinforced composites with $E_f/E_m = 1$, 10, and 100.

**15.5** Consider a carbon fiber reinforced epoxy composite. The fibers are continuous, unidirectionally aligned and 60% by volume. The tensile strength of carbon fibers is 3 GPa, and the Young's modulus is 250 GPa. The tensile strength of the epoxy matrix is 50 MPa, and its Young's modulus is 3 GPa. Compute the Young's modulus and the tensile strength of the composite in the longitudinal direction.

**15.6** A steel wire of diameter 1.25 mm has an aluminum coating such that the composite wire has a diameter of 2.50 mm. Some other pertinent data

are as follows:

| Property | Steel | Aluminum |
|---|---|---|
| Elastic modulus $E$ | 210 GPa | 70 GPa |
| Yield stress $\sigma_y$ | 200 MPa | 70 MPa |
| Poisson ratio $\nu$ | 0.3 | 0.3 |
| Coefficient of thermal expansion (linear) | $11 \times 10^{-6}$ K$^{-1}$ | $23 \times 10^{-6}$ K$^{-1}$ |

**(a)** If the composite wire is loaded in tension, which of the two components will yield first? Why?
**(b)** What tensile load can the composite wire support without undergoing plastic strain?
**(c)** What is the elastic modulus of the composite wire?
**(d)** What is the coefficient of thermal expansion of the composite wire?

**15.7** A boron–aluminum composite has the following characteristics:

Unidirectional reinforcement,
Fiber volume fraction $V_f = 50\%$,
Fiber length $\ell = 0.1$ m,
Fiber diameter $d = 100$ μm,
Fiber ultimate stress $\sigma_{fu} = 3$ GPa,
Fiber strain corresponding to $\sigma_{fu}$, $e_{fu} = 0.75\%$ (uniform elongation),
Fiber Young's modulus $E_f = 415$ GPa,
Matrix shear yield stress $\tau_{ym} = 75$ MPa,
Matrix stress at $e = e_{fu}$, $\sigma'_m = 93$ MPa,
Matrix ultimate stress $\sigma_{mu} = 200$ MPa.

Compute:

**(a)** The critical fiber length $\ell_c$ for the load transfer.
**(b)** The ultimate tensile stress of the composite.
**(c)** $V_{\min}$ and $V_{crit}$ for this composite system.

**15.8** Determine Young's modulus for a steel fiber–aluminum matrix composite material, parallel and perpendicular to the fiber direction. The reinforcement steel has $E = 210$ GPa and $V_f = 0.3$, and the aluminum matrix has $E = 70$ GPa and $V_m = 0.7$.

**15.9** An injection molded composite has short, aligned fibers. The fiber volume fraction is 40%. The length and diameter of the fibers are 500 and 10 μm, respectively. Assume a square distribution of fibers in the cross section of the composite. The Young's modulus of the fiber and matrix are 230 and 3 GPa, respectively. The shear modulus of the matrix is 1 GPa. Compute the mean strength of this composite in the fiber direction.

**15.10** A glass fiber reinforced polymer matrix composite has the following characteristics:

Fiber maximum strength = 2 GPa
Interfacial shear strength = 50 MPa
Fiber radius = 10 μm.

Compute the critical fiber length for this system.

**Fig. Ex15.12**

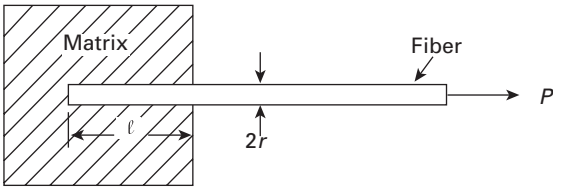


**15.11** A unidirectionally reinforced fiber reinforced composite has the following characteristics:

$E_f = 380$ GPa,
$\sigma_{fu} = 3$ GPa,
$V_f = 0.4$,
$\tau_i = 50$ MPa,
fiber length $\ell = 10$ cm,
fiber diameter $d = 15$ μm.

The matrix strength at fiber failure is = 200 MPa. Assuming that the fibers are aligned, compute the critical length for load transfer in this composite. If the load transfer coefficient $\beta = 0.5$, what is the strength of the composite along the fiber direction?

**15.12** Consider a fiber of radius $r$ embedded up to a length $\ell$ in a matrix. (See Figure Ex15.12.) When the fiber is pulled, the adhesion between the fiber and the matrix produces a shear stress $\tau$ at the interface. In a composite system containing a fiber of fracture stress $\sigma_f$ equal to eight times the maximum shear stress $\tau_{max}$ that the interface can bear, what fiber aspect ratio is required to break the fiber rather than pull it out?

**15.13** List some nonstructural applications of composite materials.[13]

**15.14** Bone is an excellent example of a natural composite. Describe the various components that make this composite.

**15.15** Describe mechanical characteristics of bone and its ability to repair.

**15.16** A glass fiber reinforced polypropylene composite has 65% by volume of fibers unidirectionally aligned.

**(a)** Compute the weight fraction of glass fibers in this composite.
**(b)** What is the density of this composite?
**(c)** Compute the Young's modulus of the composite in a direction along the fiber and perpendicular to it.

**15.17** A composite is made of unidirectional carbon fibers embedded in an epoxy matrix.

**(a)** Plot the Young's modulus as a function of the volume fraction of fibers parallel and perpendicular to the fiber direction.
**(b)** If the continuous fibers are replaced by chopped fibers with random orientation, where do you expect that the elastic properties would lie? Indicate in the plot, given $E_f = 390$ GPa; $E_m = 3$ GPa.
**(c)** Name three applications for this composite.

[13] See M. B. Bever, P. E. Duwez, and W. A. Tiller, *Mater. Sci. Eng.*, 6 (1970) 149.

**15.18** A carbon fiber–epoxy composite has 70% fibers. Determine the elastic modulus of composite along the perpendicular to fiber direction. Compute the density of this composite.

Given:

Density of carbon fibers = 1.3 g/cm$^3$,
Density of epoxy = 1.1 g/cm$^3$,
$E_c$ = 270 GPa,
$E_e$ = 4 GPa.

**15.19** A composite is made with discontinouous alumina fibers in an aluminum matrix. The fibers have a diameter of 10 μm. If the volume fraction of fibers is 60%, what is the required length if we want the strength of composite to be equal to 50% of the same composite reinforced with continuous fibers.

Given:

Fiber $E$ = 380 GPa,
Fiber strength = 1.7 GPa,
Matrix strength = 200 MPa.

**15.20** A unidirectional reinforced composite has an aluminum matrix and steel fibers (40 vol.%). Determine its strength.

Given:

Aluminum: $\sigma = 100 + \varepsilon^{0.3}$ (in MPa),
Steel: $\sigma$= 2.5 GPa.

**15.21** Describe five applications of composites in sports equipment. Specify components of the composite.

**15.22** Metals can be joined by welding, riveting, and bolting. Is it possible to apply these processes to polymer matrix composites? Explain why, and present alternative means of joining composites.

**15.23** Give specific examples for the four different types of composites, and explain briefly the components involved (e.g. particle reinforced; short fiber reinforced, etc.).

**15.24** Give an example of a composite. Compare its mechanical properties with those of the reinforcements and matrix materials, respectively, and explain its advantages.

**15.25** Consider a steel and rayon-cord reinforced elastomer (rubber) with elastic moduli as shown in the table below.

| Material | $E$ (MPa) |
|---|---|
| Rubber | 13 |
| Rayon | 6,000 |
| Steel | 210,000 |

Calculate the elastic modulus for the two different composites, if the volume fraction of fiber (rayon or steel) is 0.3.

**15.26** Consider an elastomer matrix composite reinforced with steel cord (1 mm length and 0.5 mm diameter). What is the minimum fracture stress for the steel cord, if the interfacial shear strength is 20 MPa?

**15.27** Consider an aluminum–titanium laminated composite. Calculate the longitudinal and transverse Young's modulus of this composite if the volume fractions of the two metals are equal. Given $E(\text{Ti}) = 116$ GPa, $E(\text{Al}) = 70$ GPa.

Chapter 16

# Environmental Effects

## 16.1 Introduction

Environment by its omnipresence, except perhaps in space, affects the behavior of all materials. Such effects can range from swelling in polymers to surface oxidation of metals and nonoxide ceramics to catastrophic failure of some materials under a combined action of stress and environment. Environmental degradation of materials is often referred to as corrosion. Such damage is generally time-dependent, i.e., one is able to predict it. Over time, however, environmental damage can become critical. There is, however, a more insidious corrosion problem which is time-independent. Examples of time-independent corrosion include stress corrosion cracking (SCC), environment induced embrittlement, etc. Such damage can occur at anytime, without much warning. There are many examples of such failures resulting in human and economic loss. Corrosion of structural components in aging aircraft is a serious problem. Just to cite one such example, a Boeing 737 belonging to Aloha Airlines, which flew inter island in Hawaii, lost a large portion of its upper fuselage at 7,500 m (24,000 feet) in the air. It turned out that the fuselage panels joined by rivets had corroded, which resulted in the mid-flight failure due to corrosion fatigue.

All materials (metals, ceramics, and polymers) show phenomena of premature failure or mechanical property degradation under certain combinations of stress and environment. We describe below the salient points in regard to environmental effects in different materials. We emphasize the role that the microstructure of a given material plays in this phenomenon, especially in environmentally assisted fracture.

## 16.2 Electrochemical Nature of Corrosion in Metals

Corrosion in metals, i.e., attack by an aggressive environment, is essentially electrochemical in nature. Fundamentally, there are two

**Table 16.1** | Galvanic Series of Some Metals and Alloys (in Seawater).

| | |
|---|---|
| Pt | ↑Cathodic |
| Au | |
| Graphite | |
| Ti | |
| Stainless steel (passivated) | |
| Cu–Ni alloys | |
| Bronze (Cu–Sn alloys) | |
| Cu | |
| Sn | |
| Pb | |
| Pb–Sn solders | |
| Stainless steel (activated) | |
| Cast Iron | |
| Steel | |
| Al alloys | |
| Al | |
| Zn | |
| Mg | ↓Anodic |

electrochemical reactions involved in the corrosion of a metal: oxidation and reduction. The reaction at the less noble metal is called oxidation or an anodic reaction (electrons are released in this reaction). In this case, the metal is the anode and it gets oxidized to an ion. We can write the reaction as:

$$\mathrm{M} \rightarrow \mathrm{M}^{n+} + ne^{-}.$$

At the more noble metal, one or more reduction or cathodic reactions, depending on the environment, can occur. Electrons are consumed in a cathodic reaction as per the following reaction:

$$\mathrm{M}^{n+} + ne^{-} \rightleftarrows \mathrm{M}.$$

Both these reactions occur simultaneously and at the same rate. If that were not so, there would occur a charge buildup in the metal.

One can classify the corrosion of metals in the following categories.

### 16.2.1 Galvanic Corrosion

Consider two different metals, say iron and copper, in electrical contact and exposed to an environment (i.e., an electrolyte such as water). The two dissimilar metals are said to form a *galvanic* cell. Metals and alloys can be conveniently ranked in terms of their relative reactivities to each other in an environment. Such a ranking is called the galvanic series. Table 16.1 lists some metals and alloys in the seawater environment. The metal that is less noble will corrode at the junction while the more noble one will be protected. In the example, iron will

corrode when it forms a galvanic cell with copper. The reader should note that the less noble metal is sacrificed.

Examples of such galvanic corrosion include steel screws suffering corrosion when in contact with brass in a marine environment. For example, if we have copper and steel in a water-heater, they will form a galvanic couple, and the steel will corrode. It should be pointed out that the rate of the corrosion is proportional to the ratio of the surface areas of the noble and less noble metals. Because the currents of the noble and less noble metal must be equal, therefore, if the less noble metal has a smaller surface area it will corrode very rapidly.

As a practical matter, we list some general recommendations to reduce galvanic corrosion.

- If dissimilar metals must be coupled, choose metals with similar activity.
- Avoid a small anode area.
- Electrically insulate the two metals.
- Use cathodic protection. This involves the use of a third metal that may be deliberately sacrificed. The less noble metal can be used as a sacrificial node to protect pipelines, ships, tanks, etc.

Stainless steels (Fe + Ni + 12% or more Cr) owe their corrosion resistance to a protective layer of chromium oxide. Such a coating protects the underlying metal from further corrosion.

### 16.2.2 Uniform Corrosion

This type of corrosion occurs uniformly over the entire surface. Uniform corrosion is the least objectionable corrosion form because it is easy to predict. Examples of uniform corrosion include rusting of steel and tarnishing of silver. When iron is exposed to moist air, it corrodes. This is generally referred to as "rusting." The following chemical reactions are involved in rusting:

$$\mathrm{Fe} + {}^{1}\!/_{2}\ \mathrm{O_2} + \mathrm{H_2O} \rightarrow \mathrm{Fe(OH)_2},$$
$$2\,\mathrm{Fe(OH)_2} + {}^{1}\!/_{2}\ \mathrm{O_2} + \mathrm{H_2O} \rightarrow 2\ \mathrm{Fe(OH)_3}.$$

The rust consists of $Fe(OH)_3$, a hydrated oxide, which is cathodic in nature and insoluble in water.

### 16.2.3 Crevice corrosion

Initially metal corrodes uniformly. However, if there are holes on the surface for any reason, then solution in holes is stagnant so the oxygen concentration in the crevice solution is reduced by the following reactions:

$$\mathrm{O_2} + 4\mathrm{H^+} + 4\mathrm{e^-} \rightarrow 2\mathrm{H_2O}$$

for an acidic solution containing dissolved oxygen;

$$\mathrm{O_2} + 2\mathrm{H_2O} + 4\mathrm{e^-} \rightarrow 4(\mathrm{OH})^-$$

for neutral or basic solutions with dissolved oxygen.

This generates a potential difference between crevice and non-crevice regions, also called oxygen-concentration cells. The metal in contact with the most concentrated solution is the cathode and the metal in contact with the dilute solution (in the crevice) is the anode. The crevice (crack, depression, or a dent), where the oxygen concentration is relatively low, will corrode preferentially.

To reduce crevice corrosion, one should

- Avoid crevices in design, for example use welds rather than rivets.
- Flush crevices regularly.

### 16.2.4 Pitting Corrosion

This is another form of localized corrosion that involves the formation of small pits on the surface of a metal. Pits are likely to start at structural and/or compositional heterogeneities.

### 16.2.5 Intergranular Corrosion

This type of corrosion, as suggested by the name, occurs along the grain boundaries. Generally, grain boundaries are energetically more active (i.e., anodic) than the grain interior. Recall that grain boundaries are regions of atomic disorder. Hence when exposed to an electrolyte the anodic grain boundaries dissolve preferentially and form a groove. A well known example of this is the phenomenon of *sensitization* in austenitic stainless steels. If austenitic stainless steels are heated to 500–800 °C for a long enough period, chromium carbide, $Cr_{23}C_6$, precipitates along grain boundaries. (See Figure 16.1.) This leaves the areas adjacent to the grain boundaries depleted in chromium. One needs at least 12% chromium for the stainless steel to be corrosion resistant. If the chromium content in regions adjacent to boundary falls below 12%, it will corrode preferentially. Some high strength aluminum alloys also show intergranular corrosion.

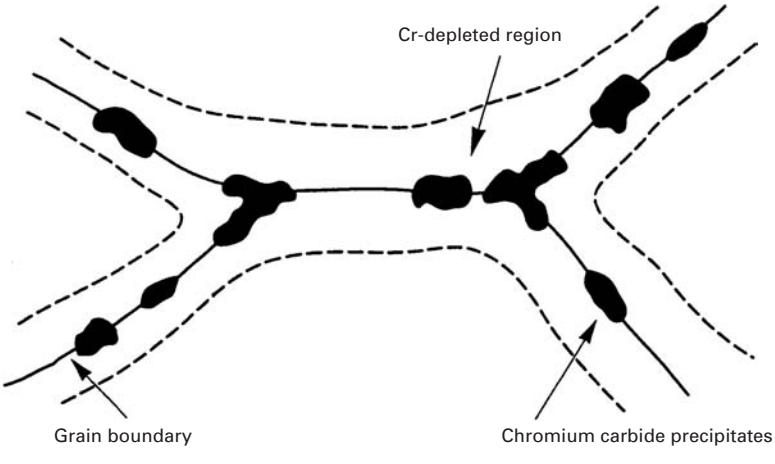


**Fig. 16.1** Sensitization of austenitic stainless steel. When austenitic stainless steels are heated to 500–800 °C for a long enough period, chromium carbide, $Cr_{23}C_6$, precipitates along grain boundaries, leaving the areas adjacent to the grain boundaries depleted in chromium and prone to corrosion.

### 16.2.6 Selective leaching

In this case, one element in an alloy dissolves preferentially. For example, zinc can leach out preferentially in a Cu–Zn brass.

### 16.2.7 Erosion-Corrosion

This type of corrosion involves a combination of chemical attack and mechanical abrasion, which is worse than either alone.

### 16.2.8 Radiation Damage

Damage can occur in metals when they are bombarded with energetic particles such as neutrons. Such damage includes formation of point defects, voids, compositional and/or microstructural changes. We have discussed this topic in Section 4.3.4. Suffice to reiterate here that among the property changes to which radiation damage can lead are: swelling, because of void formation; embrittlement, because of the generation of defects; and accelerated creep because of the formation of voids and bubbles.

### 16.2.9 Stress Corrosion

This type of degradation of a metal involves the combined action of stress and a specific corrosive medium. Failure occurs at stresses and corrosion levels where typically it would not occur alone. Residual stresses can also cause stress corrosion cracking. We describe the phenomenon of stress corrosion cracking below (Section 16.3) in some detail because of its importance.

## 16.3 Oxidation of Metals

The transformation of a metal into an oxide is accompanied by a reduction in energy, i.e., generally there is present a thermodynamic driving force for a metal to convert to what might be called its natural state. The natural state of metals (i.e., as they are found in nature) is one of compounds such as oxides, hydroxides, carbonates, silicates, sulfides, sulfates, etc. There are, of course, exceptions such as gold and platinum, which are called noble metals! Oxidation is sometimes referred to as dry corrosion. We can represent oxidation as a chemical reaction in the following manner:

$$n\,\mathrm{M}\,(\mathrm{s}) + p\mathrm{O}_2\,(\mathrm{g}) \rightarrow \mathrm{M}_n\mathrm{O}_{2p}\,(\mathrm{s\ or\ g})$$

where M represents a metal such as aluminum or a metalloid such as silicon.

Steel, which in its simplest form is an alloy of iron and carbon, can be decarburized in an oxygen environment as per the following reaction:

$$2\mathrm{C}\,(\mathrm{in\ steel}) + \mathrm{O}_2\,(\mathrm{g}) \rightarrow 2\mathrm{CO}\,(\mathrm{g}).$$

Some normally active metals become passive, i.e., lose their chemical reactivity and become inert by the formation of a highly adherent, thin oxide film on the surface that protects the metal from further corrosion. This phenomenon is called *passivity*. Examples of metals that passivate include Cr, Ni, Ti, Al. It is the chromium oxide film on the surface of stainless steel that makes the steel *stainless*, i.e., corrosion resistant. Similarly, aluminum oxide on aluminum provides a protective film. The important factor is whether the protective oxide scale that forms on the surface is protective or not? This feature can determined by a parameter called Pilling–Bedworth ratio:

$$\text{Pilling-Bedworth ratio} = A_o \rho_o / A_m \rho_m,$$

where $A_o$ is the atomic weight of the oxide, $\rho_o$ is the density of the oxide, $A_m$ is the atomic weight of the metal, and $\rho_m$ is the density of the metal.

- For a protective oxide, the Pilling–Bedworth ratio is approximately 1.
- For a porous oxide, the Pilling–Bedworth ratio is less than 1.
- For a flaking oxide, the Pilling–Bedworth ratio is around 2 to 3.

Thermal mismatch between a metal and its oxide as represented by the difference in their coefficients of thermal expansion ($\alpha_{oxide} - \alpha_{metal}$) is another important parameter.

If $\alpha_{oxide} > \alpha_{metal}$, the oxide will contract more than the underlying metal on cooling, putting the oxide layer in tension, which may crack. If $\alpha_{metal} > \alpha_{oxide}$, the metal substrate will contract more than the oxide on cooling, putting the oxide in compression, which may cause cracking or buckling of oxide and possible delamination.

If a continuous and adherent oxide film forms on the surface of a material in sufficient quantity to cover the surface, it may be used to protect the underlying material against further oxidation.

## 16.4 Environmentally Assisted Fracture in Metals

Environmentally assisted fracture in metals can be classified under the following subheadings:

- stress corrosion cracking
- hydrogen damage
- liquid and solid metal embrittlement.

### 16.4.1 Stress Corrosion Cracking (SCC)

Generally, SCC is initiated by a rupture of the protective oxide film on the metal. This film rupture may occur because of a mechanical action or a chemical action of some species. Possible initiation sites of SCC include microscopic inhomogeneities such as local differences in

**Table 16.2** Some Important Alloy–Environment Combinations for SCC

| Alloys | Environments |
|---|---|
| Copper alloys | Ammonia, sulfur dioxide, oxygen |
| Austenitic stainless steels, Al alloys, Ti alloys, high strength steels | Chlorides and moisture |
| Low carbon steels | Hydrogen sulfide |
| Carbon steels | CO or $CO_2$ and moisture |
| Copper alloys | Oxides of nitrogen |

chemical composition, amount of the corrosive species, and/or thickness of the protective film; and any stress concentration sites such as a preexisting gouge mark on the surface. Corrosion pits form at the rupture sites and cracking starts at the root of the pit. Electrochemical action maintains the sharpness of the crack tip, with corrosion continuing at the tip of a propagating crack. Bare metal under the protective film or passivated layer is exposed by the slip (i.e., plastic deformation) occurring at the crack tip. The new metal surface that is exposed becomes anodic with respect to adjacent areas that act cathodically. The corroding metal gets passivated again and the process of crack growth is repeated. The crack thus propagates in a stepwise manner in a transgranular or intergranular mode depending on the metal and environmental conditions. Characteristically, SCC shows branching, with the main crack growing in a direction perpendicular to the major tensile stress component and a low ductility.

As mentioned above, SCC occurs under the combined action of a tensile stress (applied or residual) and an aggressive environment. However, a specific metal–environment combination is required for SCC to occur. Examples include aluminum alloys–seawater, brass–ammonia, austenitic stainless steel–seawater, titanium–liquid nitrogen tetroxide ($N_2O_4$), etc. Table 16.2 summarizes some of the important metal–environment combinations.

The treatment of SCC in terms of linear elastic fracture mechanics (LEFM) analysis involves the use of crack-tip stress intensity factor as the dominant parameter controlling the crack growth under SCC conditions. Under a specific combination of a material and an aggressive environment, cracks can grow under a constant stress intensity factor $K$ less than $K_{Ic}$, the fracture toughness. We then define $K_{Iscc}$ as the threshold stress intensity value below which the crack propagation rate is negligible. One should add here the same warning in regard to the applicability of the linear fracture mechanics concepts as was done in the case of ordinary fracture in the absence of an aggressive environment; that is the size of the plastic zone at the crack tip must be small compared to the specimen dimensions for the application of LEFM to be valid. Crack growth velocity varies with the stress intensity factor, $K$. A schematic plot of log $da/dt$ vs. applied

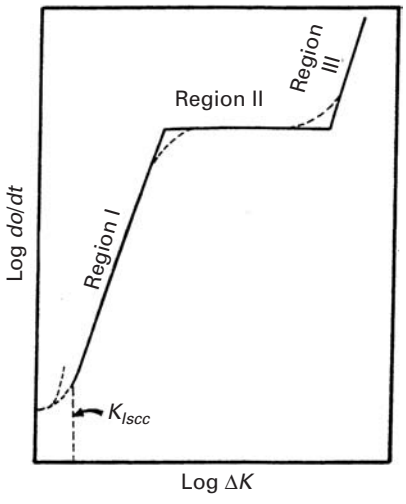


**Fig. 16.2** Crack growth rate as function of the stress intensity factor under conditions of SCC.

stress intensity is shown in Figure 16.2. There are three regions in this curve:

Region I: In this region the crack velocity depends on the stress intensity factor. The threshold stress intensity, $K_{Iscc}$, below which the crack growth does not occur, is shown by a dashed line. Quite frequently, a true $K_{Iscc}$ does not exist. In such a case, we can define an operational $K_{Iscc}$ as that corresponding to a crack growth rate of $10^{-9}$ or $10^{-10}$ ms$^{-1}$. Such an arbitrary value can be used to rate different alloys.

Region II: The crack velocity in this region is independent of the stress intensity factor. The value at which this plateau region occurs is very specific to metal/environment combination and test conditions such as temperature.

Region III: In this region the crack velocity becomes very fast as the crack-tip stress intensity factor approaches $K_{Ic}$. In this region, the crack velocity is mainly controlled by the stress intensity.

Figure 16.3 shows actual plots of log crack velocity vs. stress intensity factor for aluminum 7079 alloy in a potassium iodide solution for different temperatures.[1] Only data from regions I and II are shown in this figure. As the temperature increases, the curves shift upward, i.e., for a given stress intensity, the crack velocity increases with temperature. It should be clear to the reader that a knowledge of the full crack velocity versus stress intensity factor curve for a specific alloy in a specific environment will provide a better evaluation of the SCC resistance of the alloy in that particular environment. Similar three-region curves may be obtained under conditions of hydrogen damage and liquid metal embrittlement.

[1] M. O. Speidel, *Met. Trans.*, 6A (1975) 631.

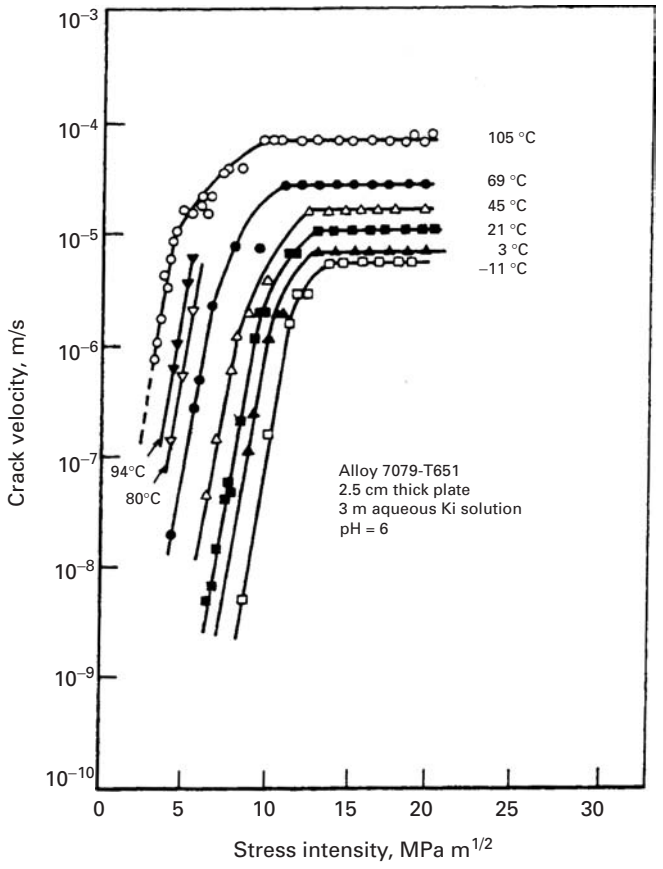


**Fig. 16.3** Log crack velocity vs. stress intensity factor for two aluminum alloys in a potassium iodide solution. Region III is not shown. (After M.O. Speidel, *Met. Trans*., 6A (1975) 631.)

**Effect of Material Variables on SCC**

In general, high purity metals are less prone to SCC than alloys or impure metals. In particular, trace amounts of interstitial elements can have a very large effect. For example, nitrogen in excess of 500 ppm in austenitic stainless steel in chloride environments can be disastrous. The cracking in austenitic stainless steels is mainly transgranular, indicating that the effect of nitrogen must either be on the process of slip or the stability of the protective film. The grain size of the metal can also have a profound effect on its resistance to SCC. A smaller grain size is more resistant to SCC than a coarse one. Elongated grain structure commonly obtained in wrought aluminum alloys can cause a markedly anisotropic SCC behavior. For example, a sheet or plate of Al 7075-T6 shows high resistance against SCC when stressed in the rolling or long transverse direction but rather poor resistance against SCC in the plate thickness direction. The 7075-T7 temper, which has a lower strength than the T6 temper, can improve resistance against SCC in the through thickness direction. Generally, the aging treatment in aluminum alloys results in increasing their resistance against SCC. The 7XXX series of aluminum alloys (Al–Zn–Mg) show the best resistance against SCC when they are aged beyond the peak hardness, i.e., in the overaged condition.

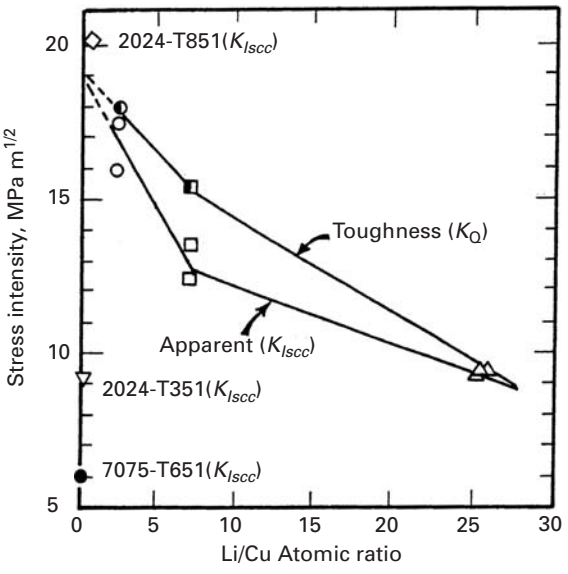


**Fig. 16.4** Decrease in $K_{Iscc}$ with increasing (Li/Cu) ratio in an Al–Li–Cu–Zr alloy (T651 temper). The apparent toughness ($K_Q$) also decreases with increasing (Li/Cu) ratio. (After A. K. Vasudevan, P. R. Ziman, S. Jha, and T. H. Sanders, in *Al-Li Alloys III* (London, The Institute of Metals, 1986), p. 303.)

Aluminum–lithium alloys are now used in the aerospace industry because of their enhanced modulus and low density (see Chapter 10). Generally, ternary or quaternary alloys are used. In particular, Al–Li–Cu–Zr alloys show quite an attractive combination of properties. It has been observed that the (Li/Cu) ratio can have significant effect on the precipitation sequence and consequently the resultant mechanical properties. The (Li/Cu) ratio also affects the stress corrosion resistance of the alloy. Figure 16.4 shows $K_{Iscc}$ in the T651 temper decreasing with increasing (Li/Cu) ratio.[2] The $K_{Iscc}$ values of 2024-T851 (peak aged) and 2024-T351 (underaged) are also included for comparative purposes. Also plotted is the apparent toughness ($K_Q$) as function of (Li/Cu) ratio. It would appear that the loss of $K_{Iscc}$ is partly due to the loss of toughness of these alloys with increasing (Li/Cu). Low-Li alloys showed the transgranular cracking and crack branching while the high-Li alloys showed intergranular cracking.

### 16.4.2 Hydrogen Damage in Metals

The presence of hydrogen in a material can cause serious damage to its performance. In addition to its great technological importance, the phenomenon of hydrogen damage has been a challenging basic research problem. One main reason for the damage caused by hydrogen in metals and alloys is the extremely small size of the hydrogen atom, which makes it move very fast in the metallic lattice. It is therefore not surprising that over the years a considerable research effort has gone into obtaining an understanding of the phenomenon, especially in metals and alloys. We provide below a short account of the hydrogen effects in various metals and alloys.

[2] A. K. Vasudevan, P. R. Ziman, S. Jha, and T. H. Sanders, in *Al-Li Alloys III* (London: The Institute of Metals, 1986), p. 303.

Some of the common sources of hydrogen in metals as well as some simple and straightforward remedies for the problem are as follows. Metals may absorb hydrogen during processing or service. For example, during melting and casting of metals, the hot metal can react with the raw materials or the humidity in air to form an oxide and hydrogen. The latter can be absorbed by the hot metal. This problem of hydrogen absorption by the liquid metal can be reduced by vacuum degassing processing. Atmospheric humidity can be a source of hydrogen in the arc welding of steels, while the electrode itself may absorb hydrogen during casting. Frequently, during some steps in the processing of a metal into a useful article, a chemical or electrochemical treatment is given. Nascent-hydrogen is released due to reaction of metal with acid during such a treatment. Most of it combines to form molecular hydrogen while the remainder will diffuse into the metal. Certain metals such as titanium, zirconium, etc. dissolve rather large quantities of hydrogen exothermally and form very brittle hydrides.

Quite frequently, in order to improve the corrosion resistance and/or for decorative purposes, electropolishing or plating of materials is carried out. Such finishing processes represent another important source of hydrogen entry into the base metal. In these finishing processes, hydrogen, together with the electroplated species, is deposited at the cathode. In such cases, it is thought by some that baking out at moderate temperatures after plating may help remove hydrogen. Others hold the view that the protective coating serves as a barrier to hydrogen removal during bakeout.

Aqueous corrosion is another common source of hydrogen for metals in service. Metal reacts with water to form an oxide (or a hydroxide) and atomic hydrogen, which is easily absorbed in the metal. In pressurized water nuclear reactors (PWR), water used for heat transfer can be an important source of hydrogen. Hydrogen embrittlement of zirconium alloy fuel cladding or of the pressure vessel itself can be a serious problem.

In the chemical and petrochemical industry, containers of chemicals (used for storage or as reaction chambers) can absorb hydrogen over a period of use. Natural gas containing $H_2S$, called sour gas, can cause hydrogen-induced cracking (HIC) in the pipeline steel. The sulfide ion is especially a problem species because it acts as a "surface poison" retarding the recombination of atomic hydrogen to form molecular hydrogen at the surface, leading to absorption of atomic hydrogen.

**Theories of Hydrogen Damage**

No single model or theory is capable of explaining all the effects associated with the presence of hydrogen in different materials. However, almost all theories recognize that one of the most important attributes of hydrogen is that it diffuses very rapidly in most any material. For example, in steels hydrogen diffuses about 10 $\mu$m per second at room temperature. This fast diffusion characteristic of

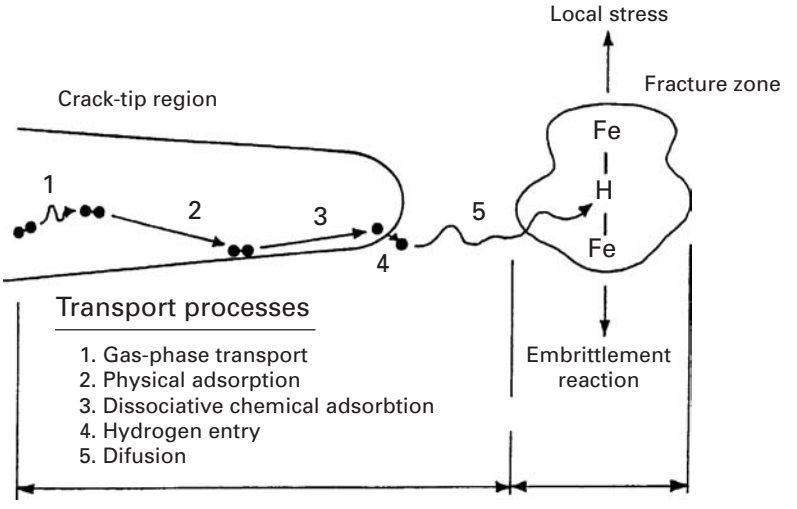


**Fig. 16.5** Schematic of the hydrogen transport processes at a crack tip in Fe and the embrittlement reaction. (After R. P. Gangloff and R. P. Wei, *Met. Trans. A*, 8A (1977) 1043.)

hydrogen stems partly from its extremely small size; hydrogen has the smallest atomic diameter among all the elements. In general, hydrogen tends to collect at defect sites in any material where it can produce high internal pressure, which can lead to cracking. There are certain special aspects of the hydrogen behavior in steels. Hydrogen has a very high mobility in the BCC lattice of Fe at ambient temperature. The comparative values of the diffusivity of hydrogen and nitrogen in the iron lattice at room temperature given below give a good idea of the extraordinarily high mobility of the hydrogen atom.[3,4]

$$D_H \text{ in Fe} \sim 10^{-2} \text{ m}^2 \text{ s}^{-1} \text{ at 300 K}$$
$$D_N \text{ in Fe} \sim 10^{-12} \text{ m}^2 \text{ s}^{-1} \text{ at 300 K.}$$

One can write for the local concentration of hydrogen in the BCC iron lattice as:[5]

$$\ln \frac{C_H}{C_0} = \frac{\Omega \sigma_p}{RT},$$

where $C_{\text{H}}$ is the local hydrogen concentration, $C_0$ is the equilibrium hydrogen concentration in the unstressed lattice, $\Omega$ is the molar volume of hydrogen in iron, $\sigma_{\text{p}}$ is the hydrostatic stress ($= \frac{\sigma_1+\sigma_2+\sigma_3}{3}$). Thus, in any nonuniformly stressed solid, there is a driving force for solute migration, which is a function of the solute atomic volume and the gradient in the hydrostatic stress component of the applied stress. Hydrogen segregates to regions of large hydrostatic tension. Figure 16.5 shows schematically the transport processes at a crack tip that eventually lead to the embrittlement reaction between the

[3] C. A. Wert, *Phys. Rev.*, 79 (1959) 601.
[4] R. A. Oriani, *in Fundamental Aspects of Stress Corrosion Cracking* (Houston, TX: NACE, 1969), p. 32.
[5] J. C. M. Li, R. A. Oriani, and L. W. Darken, *Z. Phys. Chem.* 49 (1966) 271.

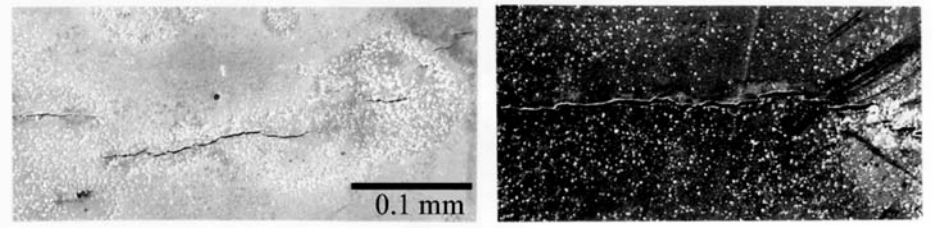


(a) (b)

**Fig. 16.6** Stepwise cracking in a microalloyed steel after 24 h cathodic charging. (From K. K. Chawla, J. M. Rigsbee, and J. D. Woodhouse, *J. Mater. Sci.*, 21 (1986) 3777.)

hydrogen and the metal, in this case iron.[6] This hydrogen transport process can be divided into the following steps:

- diffusion of hydrogen to the surface
- adsorption on the surface
- dissociation in the surface adsorption layer
- penetration through the surface
- diffusion into the bulk of the metal.

Having given this very general picture of the effects of hydrogen in metals, we review briefly some of the specific theories that have been advanced to explain the phenomenon of hydrogen damage.

**Lattice Decohesion**

A hydrogen-induced lattice decohesion can occur as originally proposed by Toriano.[7] Hydrogen diffuses into the triaxial tensile stress region at a crack tip, causing a localized reduction of the lattice cohesive strength. The concept is quite valid in very general terms. The exact mechanisms involved are, however, not clear.

**Pressure theory**

Hydrogen atoms combine and precipitate as molecular hydrogen and cause internal pressure. When this internal pressure exceeds a critical value, HIC occurs. Because of the extremely high mobility of hydrogen in most lattices, segregation of absorbed hydrogen to regions of high expansion in the lattice, for example, internal voids and cracks, occurs easily. Large internal pressure would enhance void growth and crack propagation. A good example of this phenomenon is the blister formation in steels on cathodic charging. One would expect such cracking to vary with inclusion distribution. Figure 16.6 shows such hydrogen induced cracking in a microalloyed steel sample.[8] This extensive stepwise cracking resulted after cathodic charging for 24 hours. Such cracking or voiding is frequently associated with the presence of inclusions. Figure 16.7 shows an aluminum-based inclusion (possibly alumina) in the interior of a void produced by hydrogen charging.[8] The micrograph on the right in Figure 16.7 shows the mapping of aluminum, indicating an aluminum-based inclusion.

[6] R. P. Gangloff and R. P. Wei, *Met. Trans.*, 8A (1977) 1043.
[7] A. R. Toriano, *Trans. ASM*, 52 (1960) 54.
[8] K. K. Chawla, J. M. Rigsbee, and J. D. Woodhouse, *J. Mater. Sci.*, 21 (1986) 3777.

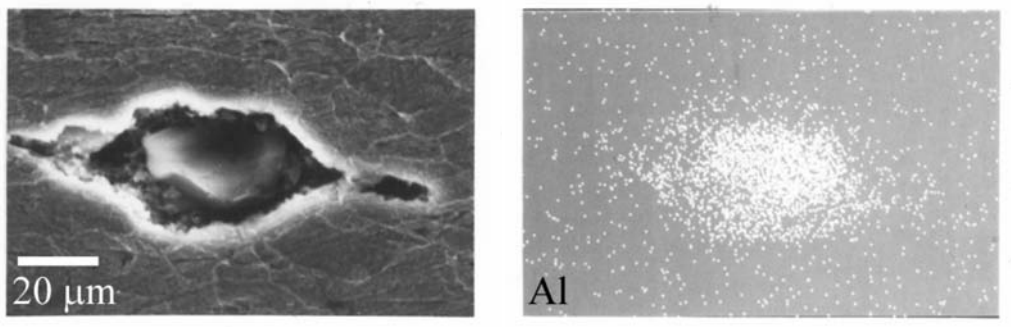


(a) ( b)

**Fig. 16.7** An aluminum-based inclusion in the interior of a void produced by hydrogen charging. (From K. K. Chawla, J. M. Rigsbee, and J. D. Woodhouse, *J. Mater. Sci.*, 21 (1986) 3777.)

The solubility of hydrogen is greatly influenced by the presence of lattice defects and impurities. For example, the solubility of hydrogen in a commercial steel at room temperature can be as much as 100% greater than that in a clean and well-annealed steel. Thus, although the solubility of hydrogen in iron is small, a large amount of it can be trapped rather easily at various defect sites.

Gas or oil containing $H_2S$ can lead to sulfide stress corrosion cracking or hydrogen induced blistering in steel.[9,10] This form of HIC, also called *blistering*, is presumed to occur when hydrogen atoms generated in a wet, sour gas environment enter into the steel and precipitate at or around inclusions or other unfavorable microstructural sites. In this regard, manganese sulfide inclusions, elongated in the rolling direction, are perhaps the worst culprits. Hydrogen atoms, generated at the surface, penetrate and diffuse into the steel. These atoms are trapped at matrix–inclusion interfaces and at ferrite–(pearlite + bainite + martensite–austenite) interfaces.[8] Here it is appropriate to point out an important microstructural feature of in rolled low carbon steels. It is tacitly assumed that the solute atoms in a solid solution are uniformly distributed in the matrix. More often than not, it is not the case. Indendritic segregation of solutes starts during the freezing of alloys. Specifically, in Mn–C steels interdendritic segregation of Mn, followed by rolling, can result in pronounced banding. Pearlite layers in the microstructure coincide with the Mn segregation. Such a microstructure consisting of alternate layers of ferrite and pearlite is very anisotropic and susceptible to hydrogen induced cracking. In quenched and tempered steels, even high Mn steels do not show such segregation; these steels have superior resistance to HIC.

### Surface Energy

According to this theory, hydrogen is adsorbed on the free surfaces of a crack and reduces the surface energy. This results in a decrease in

[9] D. D. J. Thomas and K. R. Doble, in *Steels for Linepipe & Pipeline Fittings* (London: The Metals Society 1983), p. 22.

[10] T. Taira and Kobayashi, in *Steels for Linepipe & Pipeline Fittings*, (London: The Metals Society, 1983), p. 170.

the work of fracture as per the Griffith criterion. This theory, however, would not explain the reversible degradation attributed to hydrogen.

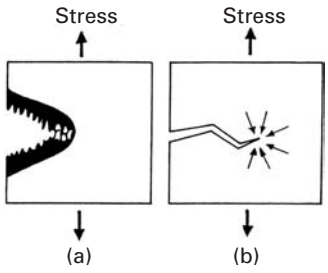


**Fig. 16.8** Schematic of crack growth in a high strength steel. (a) Without hydrogen, crack growth occurs by microvoid coalescence within a large plastic zone at the crack tip. (b) With hydrogen, plastic deformation becomes easy and crack growth occurs by severely localized deformation at the crack tip. (After C. D. Beachem, *Met. Trans*., 3A (1972) 437.)

**Enhanced Plastic Flow**

Beachem[11] proposed a hydrogen assisted cracking model in which hydrogen enhances dislocation motion. The hydrogen diffuses in front of the crack tip, increases the mobility of dislocations there and causes, locally, an enhanced plasticity. Figure 16.8 shows schematically this model. In the absence of hydrogen, a ductile metal fractures by microvoid coalescence within a large plastic zone at the crack tip, see Chapter 8. In the presence of hydrogen, however, locally plastic deformation becomes easier and crack growth occurs by severely localized deformation at the crack tip. This model has been supported experimentally by the work of Tabata and Birnbaum.[12,13] They used an *in situ* deformation stage in an environmental cell of a high voltage transmission electron microscope to investigate the effects of hydrogen on the behavior of dislocations in iron. It was observed that the introduction of hydrogen into the environmental cell increased the velocity of screw dislocations. This resulted in softening of the specimen in the early stages of deformation as the density of the mobile dislocations increased. In the later stages of deformation, this higher dislocation density may also contribute to work-hardening. These authors also studied the *in situ* fracture behavior of iron of different purities in the presence of hydrogen gas and observed that the presence of hydrogen enhanced fracture. The main conclusions of this work of are:

- Basic fracture mechanisms in iron in vacuum and in hydrogen atmosphere are the same, but the morphology of fracture is very different.
- Hydrogen enhanced fracture is caused by the localization of plasticity and by the enhancement of dislocation motion and generation in the presence of hydrogen, as first suggested by Beachem.[11]

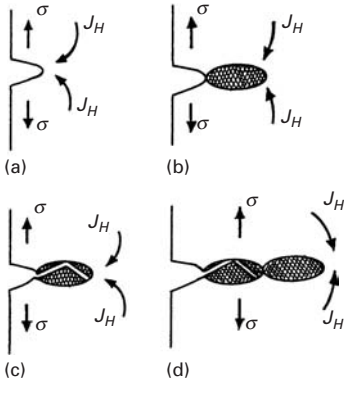


**Fig. 16.9** Hydrogen degradation due to a hydride formation. (a) Under stress, $\sigma$, hydrogen diffuses indicated by flux $J_H$, to the crack tip. (b) A hydride phase forms at the crack tip. (c) The brittle hydride phase cracks easily on continued loading. (d) New hydride phase forms and the cycle is repeated. (After H. K. Birnbaum, in *Atomistics of Fracture* (New York, Plenum, 1983), p. 733.)

**Hydride Formation**

Certain metals such as Ti, Zr, V, Nb, Ta, Mg, Al, etc. could suffer hydrogen degradation by diffusion of hydrogen and reaction with the metal to form a hydride at the crack tip. The hydride phase, being brittle, cracks easily on continued loading. Crack arrest occurs when the crack tip reaches the matrix phase. New hydride phase forms and the cycle is repeated as shown schematically in Figure 16.9.[14] In pure iron, carbon and low alloy steels, a hydride phase is not formed or is unstable. This is attributed to the extremely low solubility of hydrogen in iron and steels. Other nonhydride forming systems include Mo, W, Cr, and their alloys.

[11] C. D. Beachem, *Met. Trans*., 3A (1972) 437.
[12] T. Tabata and H. K. Birnbaum, *Scripta. Met*., 17 (1983) 947.
[13] T. Tabata and H. K. Birnbaum, *Scripta Met*., 18 (1984) 231.
[14] H. K. Birnbaum, in *Atomistics of Fracture*, (New York: Plenum, 1983), p. 733.

**Alleviating the Hydrogen Damage**

While it is very difficult to provide simple recipes for alleviating the hydrogen damage in all the materials, we may list the following general guidelines as possible solutions:

- *Avoid entry of hydrogen*. This involves a control of the external environment, i.e., use of inhibitors or suitable alloying elements to protect the base metal surfaces against hydrogen ion discharge reaction.
- *Improve the material resistance to hydrogen damage*. An effective way of doing this is to modify the morphology and/or decrease the number of inclusions. Lowering the sulfur content (maximum S about 0.010%) is a very important item in inclusion content control. Because the elongated inclusions such as MnS stringers in steel are highly susceptible to hydrogen damage, inclusion shape control through use of rare earth metals is of great help. Modifying the alloy composition is yet another way. For example, chromium as an alloying element is very beneficial in steels. The reasons for this effect may be varied. The addition of chromium decreases the solubility of hydrogen in steels, perhaps, because chromium alters the electrochemical conditions on the surface of steel, enhances the oxidation of sulfur, or depresses adsorption of atomic hydrogen.

### 16.4.3 Liquid and Solid Metal Embrittlement

Metals that fail in a ductile manner under normal conditions can fail in a very brittle fashion in the presence of certain active liquid or solid environments. This phenomenon has been variously referred to as *metal induced embrittlement* (MIE), *solid metal embrittlement* (SME), and *liquid metal embrittlement* (LME). LME of brasses and bronzes by mercury is a well known example. Gallium, which is a liquid at room temperature, causes a catastrophic failure in aluminum without any apparent diffusion. Carbon and low alloy steels are embrittled by cadmium. Amorphous metals are generally known to show excellent corrosion resistance, primarily because of the absence of grain boundaries and other defect sites. It has been observed, however, that several iron-based amorphous alloys show LME in the presence of Hg, Hg–In, or $Sn_6Pb_4$.[15]

LME is different from SCC in that positively and negatively charged ions in aqueous solution interact with solid metal in the SCC while, apparently, no electrochemical dissolution is involved in LME. There are certain prerequisites for LME to occur. The metals involved do not form any stable intermetallic compounds. The liquid metal must wet the solid metal and the metals do not have mutual solubilty.

Among the models proposed to explain the phenomenon of LME are: reduction in surface energy of the solid metal by the

[15] S. Ashok, N. S. Stoloff, M. E. Glicksman, and T. Slayin, *Scripta Met*., 15 (1981) 331.

adsorbing liquid metal species[16] and localized reduction of the strength of the atomic bonds at the crack tip by the embrittling species.[16,17] It would appear, however, that similar to the hydrogen effects in metals and alloys, different mechanisms seem to be responsible for LME under different conditions. For example, LME of many crystalline metals can be explained satisfactorily by enhanced shear or decohesion while solid metal induced embrittlement is accomplished by grain boundary penetration by the embrittling species. LME of amorphous metals, on the other hand, involves enhanced shear.

Finally, it should be pointed out to the reader that although the phenomenon of LME is generally considered as something undesirable, it is possible to use liquid metals, such as Pb–Sn eutectics, to facilitate drilling steels, titanium alloys, heat resistant Ni–Cr alloys. Increased drilling tool life and a better quality of the machined surface are improvements. Such beneficial effects have been known in nonmetallic fields for quite some time. For example, in the drilling of quartz rock, addition of $AlCl_3$ to the water lubricant allows one to double the drilling speed without increasing the wear of the drilling bit.

## 16.5 Environmental Effects in Polymers

Polymers can undergo a variety of changes due to environment, some of which can lead to severe embrittlement. Although polymers generally show good chemical resistance to various acids and alkalis, certain organic liquids and gases can affect their performance markedly. In particular, the fracture process can suffer rather drastic changes in the presence of certain environments. An example of such environmentally assisted fracture in polymers is that of polycarbonate, which fails at a low stress in a solution of sodium hydroxide in ethanol. Essentially, a specific combination of environment and stress results in a premature breakdown of the long-chain polymeric structure. Although our main concern in this section is the environmental effects on the mechanical behavior of polymers, it is worth pointing out that there is great interest in producing biodegradable polymers. This concern, of course, stems from the unsightly discarded plastic trash, which can be injurious to plant and human life. Yet another related topic, but which we shall not discuss in the book, is that of biocompatibility and stability of polymers in the body's environment, tissue–fluid interaction, etc.

Exposure to oxygen, moisture (ambient or otherwise) or other solvents, and ultraviolet radiation can lead to static fatigue or reduction in strain-to-failure. Swelling and/or dissolution are some of the most common phenomena. A liquid or solute molecule can diffuse in a polymer and cause swelling, leading to dimensional changes. Also the

[16] N. S. Stoloff and T. L. Johnston, *Acta Met.*, 11 (1963) 251.
[17] M. H. Kamdar, in Adv. in *Strength & Fracture*, Vol. l (Oxford, U.K.: Pergamon Press, 1977), p. 387.

liquid molecules push apart the chains so that secondary bonding is reduced and the polymer softens. The structural features responsible for such attack on polymers are the following.

- *Random Chain Scission*: The polymer breaks down at random points along the chain, with the attendant decrease in molecular weight and mechanical properties. The decrease in the molecular weight and/or changes the molecular weight distribution, can lead to a deterioration of the mechanical properties.
- *Successive Loss of Monomer Units*: This can occur at one extremity of the polymer chain and result in chain depolymerization. This is generally manifested in a gradual change in the molecular weight. Examples of such a phenomenon are exposure to different kinds of radiation, oxygen, ozone, etc. Rubber in the presence of ozone is particularly susceptible to this form of environmentally assisted failure. The ozone reacts at the surface of rubber and cracks nucleate and grow at low stress levels.

We provide below a brief description of different environmental effects in polymers.

### 16.5.1 Chemical or Solvent Attack

Thermoplastics can be dissolved by various organic solvents (e.g., xylene). Generally, the higher the molecular weight, $M_w$, the lower the solubility. For example, in a polymer having a distribution of various $M_w$ fractions, the low $M_w$ fractions can be dissolved and extracted by a solvent. Cross-linking of molecules, as in a thermoset, reduces solubility. Thus, a cross-linked epoxy is more resistant to chemicals than linear chain polymers such as polyethylene.

### 16.5.2 Swelling

Absorption of solvent molecules can be regarded as a form of solvent attack. Different polymers can absorb ambient moisture to different degrees. This phenomenon results in swelling of polymers and thus leads to dimensional changes. Such dimensional changes can be very important in polymers used as gaskets and seals. They also become important in polymer matrix composites, for example carbon fiber reinforced polymer. Because the polymer matrix will absorb moisture while the carbon fiber will not, there will result internal stresses due to a differential in swelling. One can get an idea of the seriousness of this problem by the following observation of carbon fiber reinforced polyimide composite. Polyimide is a high temperature polymer with a service temperature of 370 °C. However, retained moisture can result in a reduction of service temperature to 250 °C.

Generally, in monolithic polymers (i.e., not composites) swelling induced changes are reversible, i.e., the polymer will revert to its original dimensions when the absorbed molecule is removed. Moisture acts as a plasticizer, i.e., moisture absorption results in an increase impact toughness of a polymer while its strength decreases.

Swelling of a polymer can occur if a gas or a liquid permeates it. Typically, these swelling agents have small molecules and can easily penetrate the main polymeric network, where they reduce the cohesive force between the primary chains. Nylon, for example, can absorb moisture up to 1% of its weight, which can change its dimensions by about 1%. Moisture typically acts as a plasticizer, i.e., it lowers the glass transition temperature, $T_g$, of the polymer, with the result that deformation, crazing, and cracking occur at lower stress and strain values. If a polymer is uniformly swollen because of the permeation of a liquid, it will behave as a homogeneous polymer with a lower $T_g$. It should be pointed out that $T_g$ of a polymer generally varies in a nonlinear manner with the plasticizer volume fraction. Figure 16.10 shows the glass transition temperature of polymethyl methacrylate (PMMA) as a function of the volume fraction of the plasticizer diethyl phthalate.[18] The solid line in the graph is given by:

$$[T_g - T_g^*]/[T_g - T\,] = 1 + r[1 - \phi]/\phi$$

where $r = V_f/V = 0.5$, $T^*_g = -65\ ^\circ\text{C}$, $V_f$ is the free volume, $V$ is the total volume of the polymer, and the asterisks indicate the values for the plasticizer. At $\phi = 1$, $T_g = T$, as expected. The absorption of the plasticizer facilitates the molecular motion. Generally, the plasticizer has a smaller molecule size but similar chemical structure to the polymer in which it penetrates. The plasticizer molecules separate the main chains and thus reduce the intermolecular forces, i.e., their presence makes it easier for the chains to slide past one another. However, more often than not, the swelling of the polymer is not uniform, because diffusion of liquid or gas in a polymer depends on many variables, such as the size of the diffusing molecule, the microstructure of the polymer, etc. Frequently, stresses are set up at the boundary between the part penetrated by the liquid and the unpenetrated part. One can easily imagine this phenomenon to be of great concern in polymer matrix composites. In general, polymers having high bond energies, high degree of crystallinity and cross-linking, etc. will show a reduced amount of swelling.

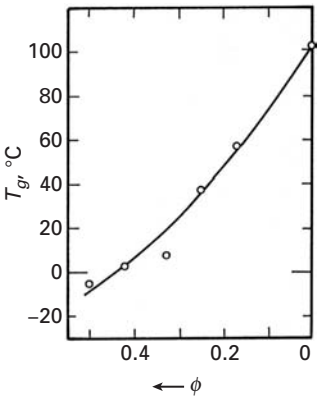


**Fig. 16.10** Decrease in glass transition temperature of polymethyl methacrylate as a function of increasing volume fraction of the plasticizer diethyl phthalate. (After F. N. Kelly and F. Bueche, *J. Polymer Sci.*, 50 (1961) 549.)

Figure 16.11 shows the decrease in tensile strength of injection-molded polyurethane when aged in distilled water at 80 °C for thirty days.[19] Initially the decrease in strength with time is slow. After ten days of exposure to water, the rate accelerates. The increase in rate of loss of strength is because of the autocatalytic nature of the hydrolysis reaction.

### 16.5.3 Oxidation

Oxidation of polymers occurs throughout their life because it is impossible to avoid interaction with the oxygen in the atmosphere.

[18] F. N. Kelly and F. Bueche, *J. Polymer Sci.*, 50 (1961) 549.

[19] D. L. Faulkner, M. G. Wyzgoski, and M. E. Myers, in *The Effects of Hostile Environments on Coatings and Plastics*, D. P. Garner and G. A. Stahl (eds), American Chemical Society, Washington, DC, 1983.

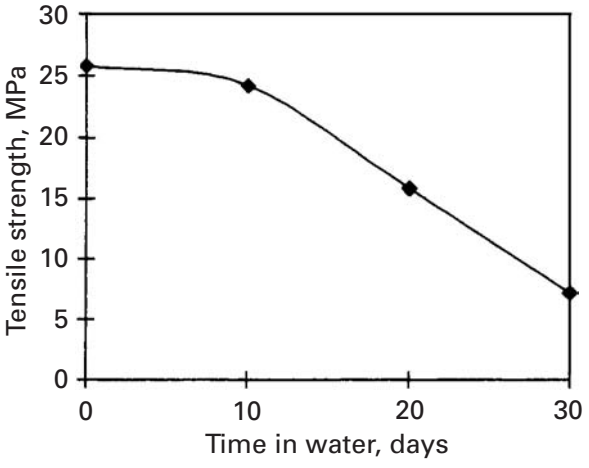


**Fig. 16.11** Tensile strength loss of polyurethane aged in water at 80 °C. (After D. L. Faulkner, M. G. Wyzgoski, and M. E. Myers, in *The Effects of Hostile Environments on Coatings and Plastics*, D. P. Garner and G. A. Stahl, eds. (Washington, DC: American Chemical Society, 1983.)

More dangerous is ozone, sometimes present in the atmosphere but always in the outer space because ozone is much more reactive than oxygen. Oxygen can permeate a polymer and increase cross-linking, thereby decreasing its toughness and flexibility. Ozone attacks any elastomer with unsaturated bonds. This is especially important in rubbers and elastomers where cracking on the surface results after prolonged exposure to air. Most of us have experienced this type damage to the sidewalls of automobile tires.

### 16.5.4 Radiation Damage

Radiation (ultraviolet, X-rays or other energetic particles such as neutrons) can lead to ionization, which can result in breaks in polymeric chains, called chain scission. (See Figure 16.12 for a schematic of this phenomenon.) Carbon–carbon (C–C) bonds form the backbone of polymers. Such bonds, however, can be ruptured by ultraviolet (UV) radiation. Rupture of molecular bonds in polymers (not in metals and ceramics) by UV radiation is commonly manifested as discoloration and loss of mechanical properties. Bond rupture can cause changes in molecular weight, degree of cross-linking, reaction with oxygen. Physical changes such as discoloration, surface embrittlement, cracking, and loss of strength are other manifestations of radiation damage in polymers. Effect of exposure to UV radiation on tensile strength of high density polyethylene is shown in Figure 16.13.[20] Tensile strength decreases with UV exposure time. UV exposure results in smaller molecules as well as a change in the molecular weight distribution, $M_w$. Consequently, mechanical properties such as strength are reduced. UV aids oxidation attack of a polymer. The term photodegradation is used to describe the damage caused by photooxidation and weathering, biodegradation, and hydrolysis. In an elastomer, there are many unsaturated double bonds along the carbon backbone.

[20] G. R. Rugger, in *Environmental Effects on Polymeric Materials*, vol. I, D. V. Rosato and R. T. Schwartz, eds. (New York: Interscience, 1968), p. 339.

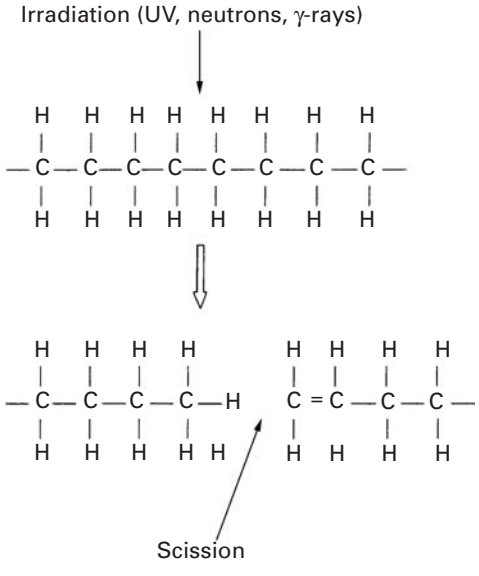


**Fig. 16.12** Effect of exposure to UV radiation on tensile strength of high density polyethylene. Tensile strength decreases with UV exposure time. (After G. R. Rugger, in *Environmental Effects on Polymeric Materials*, vol. I, D. V. Rosato and R. T. Schwartz, eds. (New York: Interscience, 1968, p. 339.)

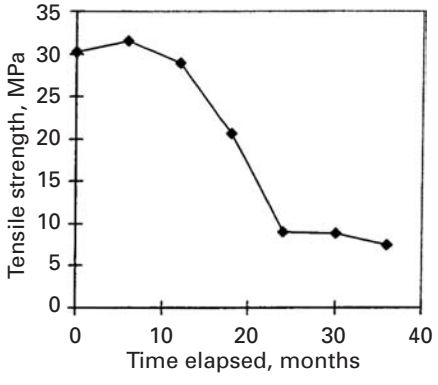


**Fig. 16.13** Decrease in tensile strength with exposure to UV radiation in high density polyethylene. (After G. R. Rugger, in *Environmental Effects on Polymeric Materials*, vol. I, D. V. Rosato and R. T. Schwartz, eds. (New York: Interscience, 1968, p. 339.)

Oxygen (or sulfur) may go to the unsaturated bond sites and provide crosslinking. Such an increase in cross-link density makes the tire strong. UV absorbing pigments (e.g., carbon black, $TiO_2$) are commonly used to alleviate this problem.

### 16.5.5 Environmental Crazing

In general, environmentally induced crazes have a faster growth rate and grow to sizes much larger than those grown in inert environments. Certain organic liquids act as crazing and cracking agents. For example, the crazes shown in Figure 8.42 in a sample of polycarbonate, were produced under dead load in a specimen of polycarbonate immersed in alcohol, which is a good crazing agent. The problem, however, is much more complex than might appear at the first sight, particularly in glassy polymers. Organic liquids which act as cracking or crazing agents can also raise the toughness of the polymer, i.e., the crack propagation rate is slowed down. For example, cracks propagate in a stable manner in PMMA in air. In the presence of methanol, a crazing agent, cracks grow in a stick–slip manner reminiscent of the

behavior of thermosetting polymers in inert environments. The stick–slip mode of crack growth occurs in thermosets because of crack blunting due to shear yielding. In PMMA, however, the crazing agent causes multiple crazing at the crack tip and blunts the crack.[21] Thus, multiple craze formation can lead to an enhanced toughness.

Although the organic liquids can cause a reduction of the surface energy, it would appear that the plasticizing effects connected with the absorption of the crazing agents into the polymer on a molecular scale are more important. Most organic liquids generally diffuse rather slowly in a bulk polymer. The same organic liquids might penetrate rapidly in a craze and plasticize it. This is because the crazed volume in a polymer is highly porous and has a high surface area to volume ratio. Even a very short diffusion time can plasticize the drawn out polymer chains in the craze, i.e., a drop in the $T_g$ will occur and it will become easier plastically to draw more polymer into fibrils at the craze surface.

### 16.5.6 Alleviating the Environmental Damage in Polymers

Additives or coatings may be introduced to thermoplastic materials to promote resistance to certain adverse environmental affects. Additives are usually introduced during the mixing and processing of thermoplastics while coatings are applied after the thermoplastic has been consolidated or processed.

Antioxidants and stabilizers are added to polymers. A well known household example is butlyated hydroxytoluol (BHT), which is added to food products to prevent oxidation. Antioxidants help a polymer retain its properties and thus provide a proper service life. Carbon black is a commonly used additive to stabilize polyolefins and other polymers against UV degradation. The UV resistance is very dependent on the amount, type, and particle size of the carbon black used. Carbon black particles of small size provide the greatest UV resistance but they tend to agglomerate into aggregates clusters.[22]

Antiozonants are additives that protect an elastomer against attack by ozone. Physical and chemical antiozonants (for example, derivatives of *p*-phenylenediamine (*p*-PDA) are used to protect rubber.

## 16.6 Environmental Effects in Ceramics

Ceramics, especially the crystalline and fully dense variety, are quite inert compared to metals and polymers. This conventional wisdom about the refractoriness of ceramics notwithstanding, it turns out that moisture can be quite a damaging species, especially to silica-based glass. For example, identical glass fibers are three times stronger when tested in vacuum than in moist air. In vacuum, freshly drawn

[21] A. J. Kinloch and R. J. Young, *Fracture Behavior of Polymers*, (London: Elsevier, 1985), p. 79.

[22] W. L. Hawkins, M. A. Worthington, and F. H. Winslow, *Rubber Age*, 88 (1960) 279.

glass fibers can show strength as high as 14 GPa, among the strongest of all materials. Exposure to ambient air for periods of two to three weeks will reduce this strength to about 5 GPa. This effect has been known for a long time. American Indians would soak their flint stones in water before fracturing them for making arrowheads. Artisans would wet scratches made into glass with saliva prior to fracturing.

Figure 16.14 shows the effect of increasing vapor pressure of water on crack propagation in a Hertzian contact fracture test on soda–lime glass.[23] This figure shows the plot of crack velocity as a function of crack extension force for different vapor pressure values. Liquid water is the most active promoter of crack growth in glass, as indicated by line *A* in Figure 16.14. As the water vapor pressure decreases, the crack velocity vs. crack extension force curves shift to the right from *B* to *E*. Not unexpectedly, different chemicals have different effects.

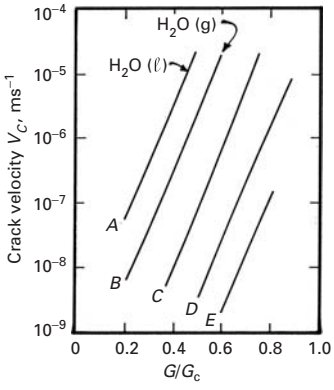


**Fig. 16.14** Crack velocity as a function of crack extension force for different vapor pressure values in a soda–lime glass. As the water vapor pressure decreases, the crack velocity vs. crack extension force curves shift to the right. Liquid water is the most active promoter of crack growth in glass, line *A*. (After M. V. Swain and B. R. Lawn, *Int. J. Fract. Mech.*, 9 (1973) 481.)

Commonly, the fall in strength as a function of time in an aggressive environment in the ceramic literature is referred to as static fatigue. Figure 16.15 illustrates the phenomenon of static fatigue for glass, i.e, failure occurs under a constant applied stress lower than the tensile stress to cause failure. The drop in strength is greater under moist conditions than under dry conditions. Mechalske and Bunker[24] studied the effect of moisture on glass in detail. The phenomenon is referred to in the literature as *stress corrosion cracking of glass*. The water molecule can penetrate to the crack tip, where it attaches itself to the silica molecules (Figure 16.16(a)). The silica molecule hydrolyzes in the presence of moisture as per

$$SiO_2 + 2H_2O \rightarrow Si(OH)_4.$$

As described in Chapter 1, the silica tetrahedra are the basic building blocks of the structure of glass. The water molecule, shown floating at the crack tip, attaches itself to two silica tetrahedra (Figure 16.16(b)). This decreases the bond strength of silica by about 20-fold and allows a much smaller applied stress to break the ring of silica tetrahedra. The process repeats itself; with water molecules penetrating the crack tip region and weakening the bonds as shown in Figure 16.16(c). A remarkable experimental evidence of this interaction of water with silica at the crack tip is shown in Figure 16.17. The low magnification optical micrograph shows a vivid proof of condensation caused by moisture at a crack tip in glass. The viscous nature of the crack-tip condensate indicates a chemical reaction between water and the glass. The effect of other molecules is not so drastic and depends on their size and reactivity.

Wiederhorn[25] modeled the effect of humidity on crack propagation velocity in a soda–lime glass. He treated the corrosion reaction at the crack tip to be an interfacially controlled process with

[23] M. V. Swain and B. R. Lawn, *Int. J. Fract. Mech.*, 9 (1973) 481.
[24] T. A. Mechalske and B. Bunker, *Sci. American*, 257 (No. 6) (1987) 122.
[25] S. M. Wiederhorn, *J. Amer. Ceram. Soc.*, 50 (1967) 407.

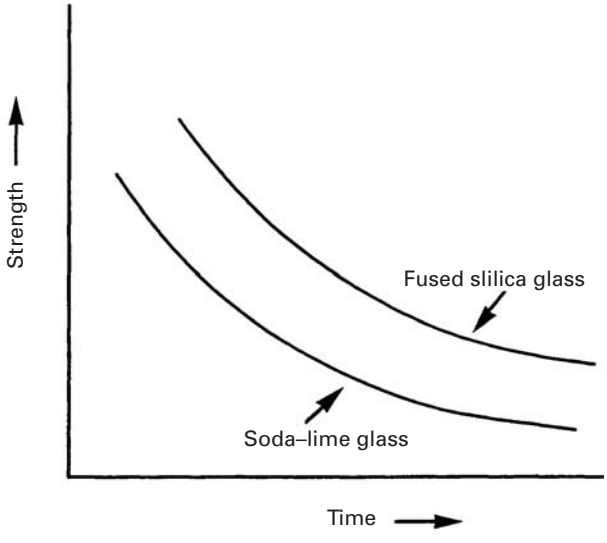


**Fig. 16.15** Schematic of static fatigue in fused silica and soda–lime glass. Although fused silica has a higher strength than soda–lime glass, both show a fall in strength as a function of time in an aggressive environment.

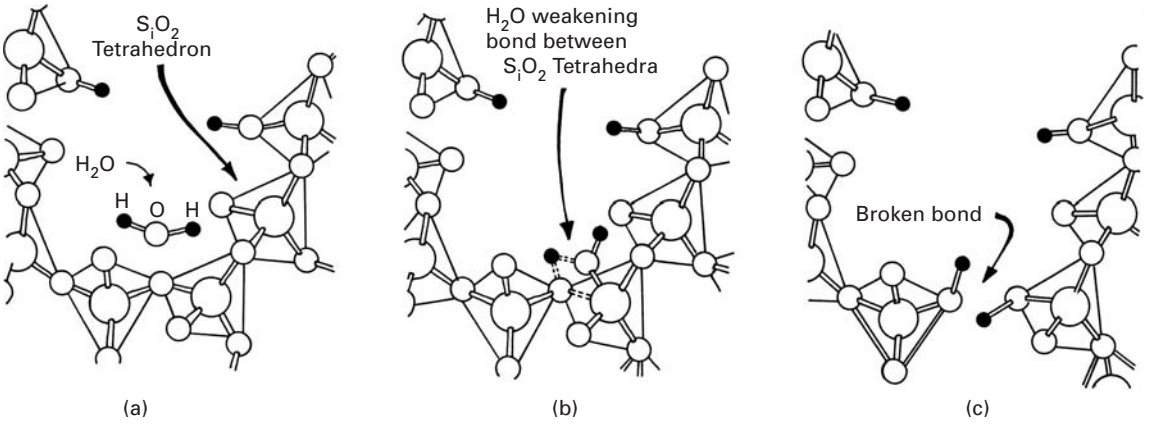


**Fig. 16.16** Interaction of the water molecule with silica at the crack tip. (a) The water molecule attaches itself to the silica molecules. (b) The water molecule, shown floating at the crack tip, attaches itself to two silica tetrahedra. (c) The process repeats itself, with water molecules penetrating the crack-tip region and weakening the bonds. (After T. A. Mechalske and B. Bunker, *Sci. American*, 257 (No. 6) (1987) 122.)

stress-dependent activation energy. The final expression for the crack velocity is

$$v = C\ \mathrm{x}^n \exp bK$$

where $C$ is the mole fraction of water vapor at the crack tip, $n$ is the number of water molecules of water reacting with a bond B:

$$n\mathrm{H_2O} + \mathrm{B} \rightarrow \mathrm{B}^*$$

and forming an activated complex $\mathrm{B}^*$. $K$ is the stress intensity factor and b is a constant. Thus, crack velocity, $v$ increases as exp $bK$ and linearly with $C$. The factor $C$ is a function of the water vapor pressure.

Alumina is also affected by the presence of moisture. Figure 16.18 shows the crack velocity as a function of applied force.[26] The test was done on a cantilever beam specimen at different relative humidities. The sapphire (single-crystal alumina) specimen was precracked along

[26] S. M. Wiederhorn, *Int. J. Fract. Mech.*, 4 (1968) 171.

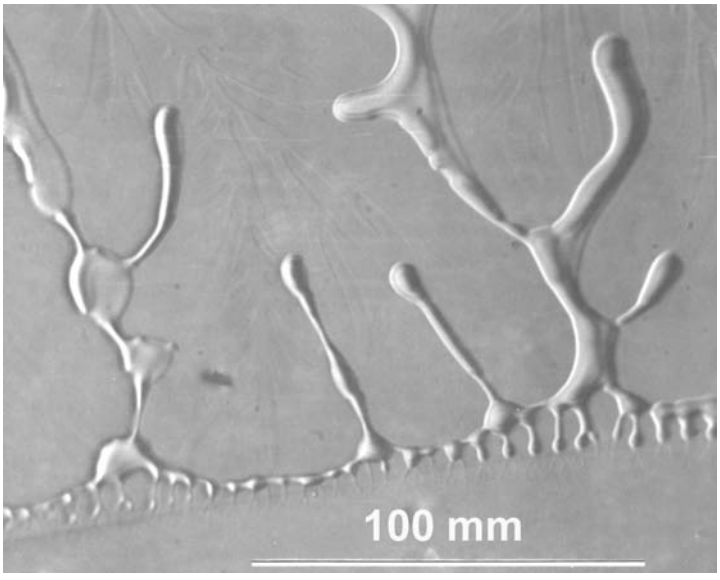


**Fig. 16.17** Condensation caused by moisture at a crack tip in glass. Note the viscous nature of the crack-tip condensate, indicating a chemical reaction between water and the glass. (Courtesy of S. Wiederhorn.)

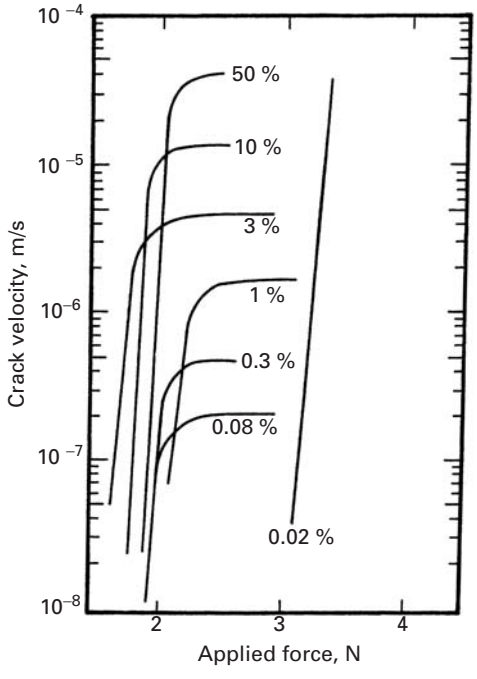


**Fig. 16.18** Crack velocity as a function of applied force in sapphire (single-crystal alumina) for different relative humidities. (After S. M. Wiederhorn, *Int. J. Fract. Mech.*, 4 (1968) 171.)

the (1011) rhombohedral plane. This is the plane that has the lowest surface energy in sapphire. The crack velocity values reach a plateau, the values of these plateaux increase with increasing humidity. The data points for 0.02% humidity are on a line that is nearly vertical.

### 16.6.1 Oxidation of Ceramics

Oxide ceramics such as alumina, mullite, silica, etc. are inherently stable in oxidizing atmospheres. That is the reason oxides such as silicates, aluminates, etc. are abundant in the earth's crust. Nonoxide

ceramics such silicon carbide, silicon nitride, molybdenum disilicide, etc. invariably have a surface layer. They tend to get oxidized at high temperatures in air.

One can represent the oxidation of structural ceramics such as SiC and $Si_3N_4$ at low oxygen partial pressures ($\leq$ 140 Pa) by the following reactions:

$$2SiC\,(s) + 3O_2\,(g) \rightarrow 2SiO\,(g) + 2CO_2\,(g),$$
$$2Si_3N_4\,(s) + 3O_2\,(g) \rightarrow 6SiO\,(g) + 4N_2\,(g).$$

In a vacuum, or an inert atmosphere, silica can degrade by

$$2SiO_2(g) \rightarrow 2SiO\,(g) + O_2\,(g).$$

Catastrophic oxidation can occur for some ceramics in the 300–700 °C range. In the literature this has been referred to as the *pesting* phenomenon. $MoSi_2$ has excellent oxidation resistance outside the pesting range because a protective layer of $SiO_2$ forms. This silica layer can protect $MoSi_2$ to 1000 °C.

## Suggested Reading

S. Al-Malaika, "Oxidative degradation and stabilisation of polymers," *Intl. Mater. Rev*., 48 (2003) 165.

H. Arup and R. N. Parkins, (eds.), *Stress Corrosion*. Alphen aan den Rijn, The Netherlands: Sijthoff & Noordhoff, 1979.

I. M. Bernstein and A. W. Thompson, eds. *Hydrogen Effects in Metals*. Warrendale, PA: TMS-AIME, 1981.

M. R. Louthan, R. P. McNitt, and R. D. Sisson, eds. *Environmental Degradation of Engineering Materials in Hydrogen*. Blacksburg, VA: Virginia Tech Printing Dept., 1981.

H. G. Nelson, in *Treatise on Materials Science and Technology*, vol. 25. New York, NY: Academic Press, 1983, p. 275.

D. Talbot and J. Talbot, *Corrosion Science and Technology*. Boca Raton, FL: CRC Press, 1998.

## Exercises

**16.1** Steel products are commonly protected by chromium or zinc coatings. Based on the galvanic series, what difference would you expect in their ability to protect steel?

**16.2** Explain why a small anode/cathode area ratio will result in a higher corrosion rate.

**16.3** Alclad aluminum consists of a thin layer (5–10% of total thickness) of one Al alloy metallurgically bonded to the core alloy. Generally, the cladding layer is anodic to the core. Why?

**16.4** Tinplate (commonly used in the canning industry) is not plate or sheet of tin. It is actually a steel strip with a thin coating of tin. Discuss the pros and cons of using tin to protect steel.

**16.5** Describe how galvanizing (coating steel with zinc) works as a cathodic protection for steel.

**16.6** Describe some methods of protecting the inside of a metallic pipe against chemical attack.

**16.7** A form of corrosion called pitting corrosion can occur in aluminum in fresh water. As the name suggests, pits form on the surface of aluminum in this type of corrosion. The pit depth, $d$ follows a cube root relationship time, $t$:

$$d = A\,t^{1/3}.$$

Normally, a 5 $\mu$m thick $Al_2O_3$ film forms on the surface of aluminum. If we double the thickness of the film, by what factor will the time to perforation increase?

**16.8** Structural ceramic materials such as SiC, $Si_3N_4$, $MoSi_2$, etc. oxidize in the presence of oxygen at high temperatures. Give the oxidation reactions and indicate how the reaction products serve to protect these materials from further oxidation. Does it have deleterious effect on the high temperature capability of these materials?

**16.9** A Ni-based superalloy has 0.2 $\mu$m thick oxide layer. When placed in a burner rig to test for oxidation, it was observed to grow to 0.3 $\mu$m in 1 h. If the superalloy follows a parabolic oxidation law ($x^2 = a + bt$, where $x$ is the thickness, $t$ is the time, and a and b are constants) what is the thickness after one week?

**16.10** The velocity of a crack in a material submerged in an aggressive medium such as humid air can be represented by:

$$V = \frac{da}{dt} = 0.5K_I^{20}.$$

Using the relationship $K_I = \sigma\sqrt{\pi a}$, compute the time to failure for this material. $K_{Ic}$ for the material is 5 MPa $m^{1/2}$.

**16.11** For a silica-based glass, the following data are available for a $V = A\,k_1^n$ type of relationship:

| Relative humidity | Preexponential constant $A$ | Crack velocity exponent $n$ |
|---|---|---|
| 10% | 2.8 | 25 |
| 100% | 4.0 | 22 |

Take $K_{Ic} = 1$ MPa $m^{1/2}$. For a crack length $a = 1$ nm, compute the fracture strength $\sigma_c$ in an inert atmosphere. Then compute the lifetime of the material under $0.3\sigma_c$ in 10% and 100% relative humidity.

**16.12** The stable, slow crack growth in a polymer in an aggressive environment can be represented by:

$$\frac{da}{dt} = 0.03K_I^2,$$

where $a$ is the crack length in meters, $t$ is the time in seconds, and $K_I$ is the stress intensity factor in MPa $m^{1/2}$. $K_{Ic}$ for this polymer is 5 MPa $m^{1/2}$. Calculate the time to failure under a constant applied stress of 50 MPa. Use $K_I = \sigma\sqrt{\pi a}$.

**16.13** It has been observed experimentally that, in cold-worked brass under stress-corrosion conditions, crack propagation is adequately described by:

$$\frac{da}{dt} = AK^2,$$

where $A$ is a constant and the other symbols have their normal significance. Derive an expression for the time to failure of the material, $t_f$, in terms of $A$, the applied stress $\sigma$, the initial crack length $a_0$, and the critical stress intensity corresponding to $a_f$ (i.e., $K_{Ic}$).

# Appendixes

| UNIT CONVERSION FACTORS | | |
|---|---|---|
| *Length* | | |
| | $1\ m = 10^{10}\ Å = 0.1\ nm$<br>$1\ mm = 0.0394\ in.$<br>$1\ cm = 0.394\ in.$<br>$1\ m = 3.28\ ft$ | $1\ Å = 10^{-10}\ m$<br>$1\ in = 25.4\ mm$<br>$1\ in = 2.54\ cm$<br>$1\ ft = 0.3048\ m$ |
| *Mass* | | |
| | $1\ Mg = 10^{3}\ kg$<br>$1\ kg = 10^{3}\ g$<br>$1\ kg = 2.205\ lb_m$<br>$1\ g = 2.205 \times 10^{-3}\ lb_m$ | $1\ kg = 10^{-3}\ Mg$<br>$1\ g = 10^{-3}\ kg$<br>$1\ lb_m = 0.4536\ kg$<br>$1\ lb_m = 453.6\ g$ |
| *Density* | | |
| | $1\ kg/m^3 = 10^{-3}\ g/cm^3$<br>$1\ kg/m^3 = 0.0624\ lb_m/ft^3$<br>$1\ g/cm^3 = 62.4\ lb_m/ft^3$<br>$1\ g/cm^3 = 0.0361\ lb_m/in.^3$ | $1\ g/cm^3 = 10^{3}\ kg/m^3$<br>$1\ lb_m/ft^3 = 16.02\ kg/m^3$<br>$1\ lb_m/ft^3 = 1.602 \times 10^{-2}\ g/cm^3$<br>$1\ lb_m/in^3 = 27.7\ g/cm^3$ |
| *Force* | | |
| | $1\ N = 10^{5}\ dynes$<br>$1\ N = 0.2248\ lb_f$ | $1\ dyne = 10^{-5}\ N$<br>$1\ lb_f = 4.448\ N$ |
| *Stress* | | |
| | $1\ MPa = 145\ psi$<br>$1\ MPa = 0.102\ kg/mm^2$<br>$1\ Pa = 10\ dynes/cm^2$<br>$1\ kg/mm^2 = 1422\ psi$ | $1\ psi = 6.90 \times 10^{-3}\ MPa$<br>$1\ kg/mm^2 = 9.806\ MPa$<br>$1\ dyne/cm^2 = 0.10\ Pa$<br>$1\ psi = 7.03 \times 10^{-4}\ kg/mm^2$ |
| *Fracture Toughness* | | |
| | $1\ psi\ in^{1/2} = 1.099 \times 10^{-3}\ MPa\ m^{1/2}$ | $1\ MPa\ m^{1/2} = 910\ psi\ in^{1/2}$ |
| *Energy* | | |
| | $1\ J = 10^{7}\ ergs$<br>$1\ J = 6.24 \times 10^{18}\ eV$<br>$1\ J = 0.239\ cal$<br>$1\ J = 9.48 \times 10^{-4}\ Btu$<br>$1\ J = 0.738\ ft\text{-}lb_f$<br>$1\ eV = 3.83 \times 10^{-20}\ cal$<br>$1\ cal = 3.97 \times 10^{-3}\ Btu$ | $1\ erg = 10^{-7}\ J$<br>$1\ eV = 1.602 \times 10^{-19}\ J$<br>$1\ cal = 4.184\ J$<br>$1\ Btu = 1054\ J$<br>$1\ ft\text{-}lb_f = 1.356\ J$<br>$1\ cal = 2.61 \times 10^{19}\ eV$<br>$1\ Btu = 252.0\ cal$ |
| *Power* | | |
| | $1\ W = 0.239\ cal/s$<br>$1\ W = 3.414\ Btu/h$<br>$1\ cal/s = 14.29\ Btu/h$ | $1\ cal/s = 4.184\ W$<br>$1\ Btu/h = 0.293\ W$<br>$1\ Btu/h = 0.070\ cal/s$ |

| UNIT CONVERSION FACTORS (*cont.*) | | |
|---|---|---|
| *Viscosity* | | |
| | 1 Pa s = 10 P | 1 P = 0.1 Pa s |
| *Temperature, T* | | |
| | $T(\text{K}) = 273 + T(^\circ\text{C})$ | $T(^\circ\text{C}) = T(\text{K}) - 273$ |
| | $T(\text{K}) = \frac{5}{9}[T(^\circ\text{F}) - 32] + 273$ | $T(^\circ\text{F}) = \frac{9}{5}[T(\text{K}) - 273] + 32$ |
| | $T(^\circ\text{C}) = \frac{5}{9}[T(^\circ\text{F}) - 32]$ | $T(^\circ\text{F}) = \frac{9}{5}[T(^\circ\text{C}) + 32]$ |
| *Specific Heat* | | |
| | 1 J/kg-K = 2.39 × $10^{-4}$ cal/g-K | 1 cal/g-°C = 4184 J/kg-K |
| | 1 J/kg-K = 2.39 × $10^{-4}$ Btu/$lb_m$-°F | 1 Btu/$lb_m$-°F = 4184 J/kg-K |
| | 1 cal/g-°C = 1.0 Btu/$lb_m$-°F | 1 Btu/$lb_m$-°F = 1.0 cal/g-K |

| STANDARD PREFIXES, SYMBOLS, AND MULTIPLICATION FACTORS | | |
|---|---|---|
| Prefix | Symbol | Factor by Which Unit Has to Be Multiplied |
| Tera | T | $10^{12}$ |
| Giga | G | $10^{9}$ |
| Mega | M | $10^{6}$ |
| Kilo | k | $10^{3}$ |
| Hecto | h | $10^{2}$ |
| Deca | da | $10^{1}$ |
| Deci | d | $10^{-1}$ |
| Centi | c | $10^{-2}$ |
| Milli | m | $10^{-3}$ |
| Micro | μ | $10^{-6}$ |
| Nano | n | $10^{-9}$ |
| Pico | p | $10^{-12}$ |
| Femto | f | $10^{-15}$ |
| Atto | a | $10^{-18}$ |

IMPORTANT CHARACTERISTICS OF SOME ELEMENTS

| Symbol | Atomic Number | Atomic Weight (amu) | Density of Solid, 20 °C ($g/cm^3$) | Crystal Structure, 20 °C | Atomic Radius (nm) | Ionic Radius (nm) | Most Common Valence | Melting Point (°C) |
|---|---|---|---|---|---|---|---|---|
| Al | 13 | 26.98 | 2.70 | FCC | 0.143 | 0.053 | 3+ | 660.4 |
| Ar | 18 | 39.95 | – | – | – | – | Inert | −189.2 |
| Ba | 56 | 137.33 | 3.5 | BCC | 0.217 | 0.136 | 2+ | 725 |
| Be | 4 | 9.012 | 1.85 | HCP | 0.114 | 0.035 | 2+ | 1278 |
| B | 5 | 10.81 | 2.34 | Rhomb. | – | 0.023 | 3+ | 2300 |
| Br | 35 | 79.90 | – | – | – | 0.196 | 1− | −7.2 |
| Cd | 48 | 112.41 | 8.65 | HCP | 0.149 | 0.095 | 2+ | 321 |
| Ca | 20 | 40.08 | 1.55 | FCC | 0.197 | 0.100 | 2+ | 839 |
| C | 6 | 12.011 | 2.25 | Hex. | 0.071 | ~0.016 | 4+ | (sublimes at 3367) |
| Cs | 55 | 132.91 | 1.87 | BCC | 0.265 | 0.170 | 1+ | 28.4 |
| Cl | 17 | 35.45 | – | – | – | 0.181 | 1− | −101 |
| Cr | 24 | 52.00 | 7.19 | BCC | 0.125 | 0.063 | 3+ | 1875 |
| Co | 27 | 58.93 | 8.9 | HCP | 0.125 | 0.072 | 2+ | 1495 |
| Cu | 29 | 63.55 | 8.96 | FCC | 0.128 | 0.096 | 1+ | 1084 |
| F | 9 | 19.00 | – | – | – | 0.133 | 1− | −220 |
| Ga | 31 | 69.72 | 5.90 | Ortho. | 0.122 | 0.062 | 3+ | 29.8 |
| Ge | 32 | 72.59 | 5.32 | Dia. cubic | 0.122 | 0.053 | 4+ | 937 |
| Au | 79 | 196.97 | 19.3 | FCC | 0.144 | 0.137 | 1+ | 1064 |
| He | 2 | 4.003 | – | – | – | – | Inert | −272 (at 26 atm) |
| H | 1 | 1.008 | – | – | – | 0.154 | 1+ | −259 |
| I | 53 | 126.91 | 4.93 | Ortho. | 0.136 | 0.220 | 1− | 114 |
| Fe | 26 | 55.85 | 7.87 | BCC | 0.124 | 0.077 | 2+ | 1538 |
| Pb | 82 | 207.2 | 11.35 | FCC | 0.175 | 0.120 | 2+ | 327 |
| Li | 3 | 6.94 | 0.534 | BCC | 0.152 | 0.068 | 1+ | 181 |
| Mg | 12 | 24.31 | 1.74 | HCP | 0.160 | 0.072 | 2+ | 649 |
| Mn | 25 | 54.94 | 7.44 | Cubic | 0.112 | 0.067 | 2+ | 1244 |
| Hg | 80 | 200.59 | – | – | – | 0.110 | 2+ | −38.8 |
| Mo | 42 | 95.94 | 10.22 | BCC | 0.136 | 0.070 | 4+ | 2617 |
| Ne | 10 | 20.18 | – | – | – | – | Inert | −248.7 |
| Ni | 28 | 58.69 | 8.90 | FCC | 0.125 | 0.069 | 2+ | 1453 |
| Nb | 41 | 92.91 | 8.57 | BCC | 0.143 | 0.069 | 5+ | 2468 |
| N | 7 | 14.007 | – | – | – | 0.01−0.02 | 5+ | −209.9 |
| O | 8 | 16.00 | – | – | – | 0.140 | 2− | −218.4 |
| P | 15 | 30.97 | 1.82 | Ortho. | 0.109 | 0.035 | 5+ | 44.1 |
| Pt | 78 | 195.08 | 21.45 | FCC | 0.139 | 0.080 | 2+ | 1772 |
| K | 19 | 39.10 | 0.862 | BCC | 0.231 | 0.138 | 1+ | 63 |
| Si | 14 | 28.09 | 2.33 | Dia. cubic | 0.118 | 0.040 | 4+ | 1410 |
| Ag | 47 | 107.87 | 10.5 | FCC | 0.144 | 0.126 | 1+ | 962 |
| Na | 11 | 22.99 | 0.971 | BCC | 0.186 | 0.102 | 1+ | 98 |
| S | 16 | 32.06 | 2.07 | Ortho. | 0.106 | 0.184 | 2− | 113 |
| Sn | 50 | 118.69 | 7.3 | Tetra. | 0.151 | 0.071 | 4+ | 232 |
| Ti | 22 | 47.88 | 4.51 | HCP | 0.145 | 0.068 | 4+ | 1668 |
| W | 74 | 183.85 | 19.3 | BCC | 0.137 | 0.070 | 4+ | 3410 |
| V | 23 | 50.94 | 6.1 | BCC | 0.132 | 0.059 | 5+ | 1890 |
| Zn | 30 | 65.39 | 7.13 | HCP | 0.133 | 0.074 | 2+ | 420 |
| Zr | 40 | 91.22 | 6.51 | HCP | 0.159 | 0.079 | 4+ | 1852 |

Adapted from W. D. Callister, *Materials Science* and Engineering. New York, NY John Wiley & Sons, 1997.

MECHANICAL PROPERTIES OF SOME IMPORTANT CERAMIC MATERIALS

| | Weibull modulus | Flexural strength (MPa) | Young's modulus (GPa) | Poisson's ratio | Compressive strength (MPa) | Hardness (HV) | Tensile strength (MPa) | Fracture toughness (MPa $m^{1/2}$) |
|---|---|---|---|---|---|---|---|---|
| Silicon Nitride | 20 | 930 | 320 | 0.28 | 2100–3500 | 1800 | 350–415 | 6 |
| Silicon Carbide | 18 | 634 | 450 | 0.17 | 1035–1725 | 2300 | 390–450 | 4.3 |
| Aluminum Nitride | 10 | 200 | 320 | 0.22 | 1400–2100 | 1110 | – | 3 |
| Tungsten Carbide | – | 1930 | 627 | 0.21 | 2683 | 1600 | 344 | – |
| Titanium Oxide | – | 137 | 228 | 0.27 | 688 | 800 | 51.6 | 3.2 |
| MgO stabilized Zirconia | – | 620 | 200 | 0.3 | 1750 | 1200 | 352 | 11 |
| Aluminum Oxide (98%) | 10 | 300 | 340 | 0.22 | 2500 | 1800 | 150 | 4 |
| Aluminum Oxide (99%) | 10 | 400 | 370 | 0.22 | 3000 | 1800 | 180 | 4 |
| Zirconia toughened alumina (ZTA) | 13 | 912 | 285 | 0.25 | – | 1500 | – | 6.9 |
| Boron Carbide | 12 | 450 | 450 | 0.27 | 470 | 2700 | – | 3.0 |
| Titanium Diboride | 11 | 277 | 556 | 0.11 | 470 | 2700 | – | 6.9 |
| Zirconia | 15 | 800–1200 | – | 0.28 | 2000 | 1200 | – | 6–8 |

Note: the values given are indicative only

MECHANICAL PROPERTIES OF SOME IMPORTANT METALS AND ALLOYS

| Alloy | Density ($kg/m^3$) | M.P. (°C) | Young's modulus (GPa) | Poisson's ratio | UTS (MPa) | Yield strength (MPa) | Strain-to-failure (%) | Fracture toughness MPa $m^{1/2}$ |
|---|---|---|---|---|---|---|---|---|
| Al 2024-T 851 | 2770 | 502 | 72.4 | 0.33 | 455 | 400 | 5 | 26.4 |
| Al 7075-T 651 | 2810 | 477 | 72 | 0.33 | 570 | 505 | 11 | 24.2 |
| Al 7178-T651 | 2830 | 477–629 | 73 | 0.33 | 605 | 540 | 10 | 23.1 |
| Ti-6Al-4V (grade 5) | 4430 | 1604–1660 | 113.8 | 0.342 | 1860 | 1480 | 14 | 55 |
| Ti-3Al-2.5V (alpha annealed) | 4480 | 1700 | 100 | 0.3 | 620 | 500 | 15 | 100 |
| 702 Zirconium | 6500 | 1852 | 99.3 | 0.35 | 379 | 207 | 16 | – |
| 60–40 Soft solder | 8600 | 183–190 | 30 | 0.4 | 53 | – | – | – |
| Stainless steel 4340 | 7850 | – | 205 | – | 745 | 470 | 22 | 60.4 |
| Stainless steel 304 | 8000 | 1400 | 193 | 0.29 | 505 | 215 | 70 | – |
| Steel 5160 | 7850 | – | 205 | – | 724 | 275 | 17.2 | – |
| Tool steel H 11 hot worked | 7800 | – | 210 | – | 1990 | 1650 | 9 | – |
| Maraging steel (18 Ni) (before aging) | 8000 | – | 183 | – | 965 | 660 | 17 | – |
| Maraging steel (18 Ni) (annealed & aged at 480 °C) | 8080 | | 200 | – | 1864 | 1737 | 17.4 | – |
| Superalloy CoCrWNi | 10000 | – | – | – | 860 | 310 | 10 | – |
| Superalloy Fe based N08330 Ni | 8000 | – | – | – | 586 | 276 | 40 | – |
| Superalloy H-X Nickel | 8220 | – | – | – | 690 | 276 | 40 | – |

Note: the values given are indicative only

MECHANICAL PROPERTIES OF SOME IMPORTANT POLYMERIC MATERIALS

| | Density ($g\ cm^{-3}$) | Young's modulus (MPa) | Tensile strength (MPa) | Strain-to-fracture (%) | Yield stress (MPa) | Yield strain | Rockwell hardness | Izod impact Energy, J/m |
|---|---|---|---|---|---|---|---|---|
| *Thermoplastics* | | | | | | | | |
| Cellulose acetate(soft) | 1.27–1.34 | 593–1723 | 13–32 | 32–50 | 15–28 | – | R49–R103 | 100–270 |
| Cellulose acetate (hard) | 1.27–1.34 | 1309–2757 | 31–58 | 6–40 | 28–52 | – | R101–R123 | 3140–5060 |
| Cellulose acetate butyrate (soft) | 1.15–1.22 | 510–868 | 13–26 | 60–74 | 8.2–17 | – | R59–R95 | 130–290 |
| Cellulose acetate butyrate (hard) | 1.19–1.25 | 1034–1378 | 34–46 | 38–54 | 24–42 | – | R108–R117 | 38–130 |
| Nylon 6/6 | 1.13–1.25 | – | 62–82 | 60–300 | – | – | R108–R120 | 50–100 |
| Polycarbonates (unfilled) | 1.2 | 2000–2240 | 55–65 | 20–100 | 55–68 | – | M70–M180 | 430–850 |
| Polyethylene (low density) | 0.91–0.925 | 96–260 | 6.9–9.6 | 400–700 | 7.5–11.7 | 20–40 | – | – |
| Polyethylene (medium density) | 0.926–0.941 | 240–620 | 8.2–24.1 | 50–600 | 10.3–17.9 | 10–20 | – | 26–850 |
| Polyethylene (high density) | 0.941–0.965 | 590–1110 | 21–37 | 15–100 | 16.5–34.4 | 5–10 | R30–R50 | 80–1050 |
| Methylmethacrylate (PMMA unmodified) | 1.18–1.20 | 2410–3450 | 48–75 | 2–10 | – | – | M80–M105 | 16–32 |
| Polypropylene (unmodified) | 0.9 | 9.65–11.8 | 29–37 | >220 | 33.8 | 15 | 93 | 53 |
| Polypropylene (copolymer) | 0.9 | – | 19–31 | 200–700 | – | – | R50–R96 | 58–64 |
| Polystyrene (unmodified) | 1.04–1.08 | 2750–4140 | 34–68 | 1–2.5 | – | – | M65–M85 | 13–32 |
| PTFE (unmodified) | 2.1–2.3 | 1030 | 31–41 | 250 | 29 | 10 | J75–J95 | 130–210 |
| *Thermosetting* | | | | | | | | |
| Epoxy (unfilled) | 1.115 | 2070 | 27–89 | 2–6 | – | – | M75–M110 | 10–50 |
| Melamine formaldehyde | 1.47–1.52 | 8960 | 48–90 | 0.6–0.9 | – | – | M110–M124 | 12–18 |
| Polyester (glass fiber mat reinforced) | 1.5–2.1 | 3450 | 206–344 | .5–1.5 | – | – | M80–M120 | 370–1600 |
| Silicones (mineral filled) | 1.8–2.8 | – | 20–27 | – | – | – | M85–M95 | 13–18 |
| Urea formaldehyde ($\alpha$-cellulose filled) | 1.47–1.52 | 8970 | 37–89 | 0.6 | – | – | E94–E97 | 12–20 |
| ABS (high-heat resistant) | 1.06–1.08 | – | 48–62 | 1–20 | 28–62 | – | R110–R115 | 100–210 |

Note: the values given are indicative only

# Index